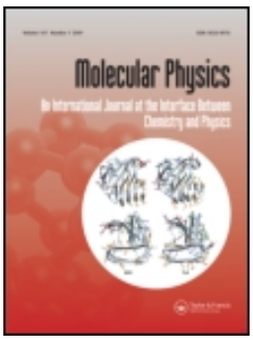

Molecular Physics

ISSN: 0026-8976 (Print) 1362-3028 (Online) Journal homepage: http://www.tandfonline.com/loi/tmph20

The structure of carbodiimide, HNCNH

WOLFGANG JABS , MANFRED WINNEWISSER , SERGEI P. BELOV , FRANK LEWEN , FRANK MAIWALD & GISBERT WINNEWISSER

To cite this article: WOLFGANG JABS , MANFRED WINNEWISSER , SERGEI P. BELOV , FRANK LEWEN , FRANK MAIWALD & GISBERT WINNEWISSER (1999) The structure of carbodiimide, HNCNH, Molecular Physics, 97:1-2, 213-238, DOI: 10.1080/00268979909482825

To link to this article: http://dx.doi.org/10.1080/00268979909482825

Published online: 01 Sep 2009.

MOLECULAR PHYSICS, 1999, VOL. 97, NO. 1/2, 213–238

The structure of carbodiimide, HNCNH

WOLFGANG JABS[1]†, MANFRED WINNEWISSER[1], SERGEI P. BELOV[2], FRANK LEWEN[2], FRANK MAIWALD[2] and GISBERT WINNEWISSER[2]

[1] Physikalisch-Chemisches Institut, Justus-Liebig-Universität, Heinrich-Buff-Ring 58, D-35392 Gießen, Germany

[2] I. Physikalisches Institut, Universität zu Köln, Zülpicherstraße 77, D-50937 Köln, Germany

(*Received 19 August 1998; revised version accepted 6 November 1998*)

An experimentally determined r_s-type structure of HNCNH is reported: $r_{NH} = 1.0074$ Å, $r_{CN} = 1.2242$ Å, $\angle HNC = 118.63°$, $\angle NCN = 170.63°$, $\angle HN\cdots NH = 88.99°$. The number of digits quoted allow for errors with two significant figures. In order to obtain these values we recorded rotational–torsional spectra of $HN^{13}CNH$, $H^{15}NC^{15}NH$ and DNCND, by using isotopically enriched cyanamide. A chemical equilibrium exists between carbodiimide, HNCNH, and the more stable isomer cyanamide, H_2NCN, which strongly favours cyanamide (approximately 1:115 at 110 °C). The expensive C- and N-substituted isotopomers could only be investigated in the millimetre wave region, while for DNCND the far infrared spectrum between 10–350 cm^{-1} was also recorded. Rotational constants of the three isotopomers, as well as of the parent species, were determined by fitting the assigned spectral transitions to the Watson Hamiltonian in S reduction. Using fitting programs written by Schwendeman and Rudolph, r_0, r_s and $r_m^{(0)}$ structures of HNCNH were derived. The experimentally determined structural parameters are compared with an *ab initio* r_e structure.

1. Introduction

Carbodiimide, HNCNH, belongs like H_2O_2 and H_2S_2 to the C_2-symmetry group and is a skew-chain molecule, as is shown in figure 1. Molecules of this type are accidentally nearly symmetric tops; for HNCNH Ray's asymmetry parameter κ was found to be $-0.999\,995\,368(18)$ [1]. The permanent electric dipole moment coincides with the C_2-symmetry axis, which is perpendicular to the axis of the least principal moment of inertia. For HNCNH the C_2 axis is the b axis, so that a perpendicular b-type rotational spectrum dominated by strong Q-branch absorptions is observed.

The H atoms of carbodiimide undergo internal rotation hindered by *cis* and *trans* potential barriers of nearly equal height, about 2070 cm^{-1}, leading to a torsional doublet splitting of all rovibrational transitions [1–5]. The large-amplitude torsional motion is accompanied by significant changes in the HNC and NCN angles, which effectively lower the torsional barriers. On the other side rotation about the a axis produces a centrifugal force which prevents the molecule from following the minimum energy torsional path, increasing the torsional potential barriers. Therefore the torsional splitting depends on K_a and the doublet splitting collapses at high K_a [1–3]. For $K_a = 0$ and 1 the torsional splitting depends also on the rotational quantum number J. Furthermore, HNCNH, like H_2S_2, shows an anomalous K_a doubling of the $K_a = 2$ rotational torsional energy levels: the levels are inverted [4].

The goal of the present work was the determination of the molecular structure of HNCNH with spectroscopic methods. The result is compared with *ab initio* calculations performed at high levels of theory parallel to the experimental work. The *ab initio* calculations are reported in a separate article [6].

The experimental structure of HNCNH was not previously determined, due to the experimental difficulties presented by a chemical equilibrium between carbodiimide and cyanamide which is strongly dominated by cyanamide. Because cyanamide also undergoes a large amplitude inversional motion, the spectrum of this species is especially dense [7].

For the experimental evaluation of the structure, rotational–torsional spectra of $HN^{13}CNH$, $H^{15}NC^{15}NH$ and DNCND were measured in the millimetre wave region. Fourier transform infrared (FTIR) spectra of the first two expensive isotopomers could not be obtained, because the sample consumption for such measurements is too high. However, the rotational–

† Part of the author's dissertation, Justus-Liebig-Universität (D26).

Molecular Physics ISSN 0026-8976 print/ISSN 1362-3028 online
http://www.tandf.co.uk/JNLS/mph.htm
http://www.taylorandfrancis.com/JNLS/mph.htm

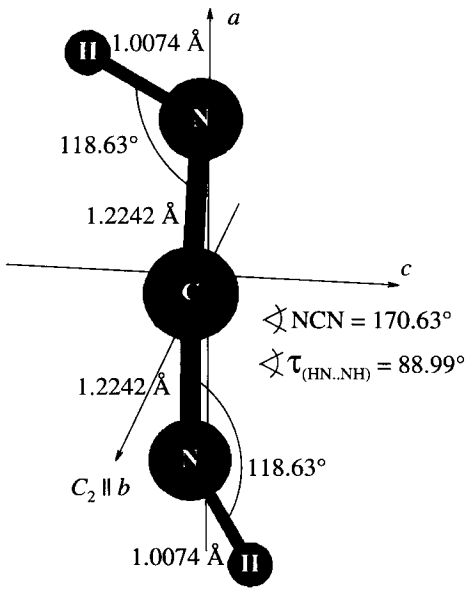

Figure 1. The carbodiimide molecule. The C_2-symmetry axis coincides with the *b* axis. The internuclear distances and bond angles of structure number 9 in table 8 (see section 5) are given. The errors of the distances are estimated to be in the range from 0.002 to 0.01 Å, and the errors of the bond angles in the range from 0.1 to 0.2° (see text).

torsional spectrum of DNCND was successfully recorded in the far infrared (FIR) region.

2. Experimental details

In order to determine the structure of HNCNH from experimental data, spectra were recorded with three different spectrometers.

2.1. *Measurements with the Cologne millimetre/submillimetre wave/terahertz spectrometer*

The essential elements of the Cologne spectrometer are high-frequency, broad-band tunable backward wave oscillators (BWOs) obtained from the ISTOK Research and Production Company, together with a subharmonic mixer, and a low-noise HEMT (high-electron mobility transistor) amplifier circuit for the intermediate frequency (IF) path. A tunable millimetre wave KVARZ synthesizer which covers the frequency region 78–118 GHz [8–10] is used to stabilize the BWO source frequency. In this study two BWOs were used, one with a frequency coverage from 258 to 375 GHz, the other one operating in the frequency region from 530 to 714 GHz. In the first region, we observed the $^rQ_0$ branches and some $^rP_0$ transitions of $H^{15}NC^{15}NH$ and $HN^{13}CNH$, while in the second region the $^rQ_1$ branch of DNCND was observed and measured.

The power output of the high frequency BWO is divided: a small fraction is used to drive the frequency stabilization system by using suitable harmonics of the output frequency of a KVARZ synthesizer. The major portion of the BWO radiation power is focused through a free space absorption cell 4 m in length onto a He-cooled InSb hot-electron bolometer. Source modulation (modulation frequency = 7 kHz, modulation deviation = 480 kHz) with second derivative detection was employed. A sample pressure of 2 Pa was maintained in the cell, at room temperature, by pumping on a commercial sample of cyanamide (melting point: 46 °C) stabilized with NaH_2PO_4. Isotopically enriched samples of $H_2^{15}NC^{15}N$ and $H_2N^{13}CN$ were obtained from Icon Services Inc. with specified enrichment of 99%. Deuterocyanamide was prepared according to a description given by Fletcher and Brown [11]: repeated solution of freshly sublimated H_2NCN in D_2O followed by evaporation under vacuum from D_2O over P_2O_5 yielded D_2NCN of approximately 90% deuteration after six exchanges. Before dissolving the H_2NCN sample for the first time in D_2O, a small amount of KD_2PO_4 was added to stabilize the deuterocyanamide.

In the gaseous phase cyanamide is in equilibrium with carbodiimide. At room temperature only $\approx 0.25\%$ of the sample exists as carbodiimide [12], so that the partial pressure of carbodiimide was of the order of 0.005 Pa. Consequently the weak spectrum of carbodiimide is interspersed among the strong absorption lines of cyanamide. The absolute accuracy of the line positions is better than 30 kHz for strong and unblended lines and 300 kHz for weak and partly blended lines.

2.2. *Measurements with the millimetre wave spectrometer in Gießen*

The AM-MSP spectrometer designed by the Analytik & Meßtechnik GmbH, Chemnitz, covers a frequency region between 52 and 179 GHz. The spectrometer consists of a millimetre wave synthesizer, a modulation unit and a receiver module. The millimetre wave power is generated by BWOs with output power levels between 1 and 25 mW. The radiation is guided through a 2.5 m glass absorption cell onto a detector. The detector consists of a silicon Schottky barrier diode at room temperature. Source modulation (modulation frequency = 200 kHz, modulation deviation = 300 kHz) was used. A detailed description of the spectrometer is given by Winnewisser *et al.* [13]. The accuracy of line positions is estimated to be ± 10 kHz for strong and unblended lines and ± 100 kHz for weak and partly blended lines.

In order to extend the available frequency range up to 600 GHz a frequency multiplier based on a planar Schottky diode was developed in the Cologne laboratory [14]. In this work the multiplier was used to generate second harmonic power to record the $^rQ_0$ branch of DNCND at 202 GHz. The radiation was detected by

Table 1. Measurement parameters for the FIR spectra of D_2NCN/DNCND.

Region /cm^{-1}	1/(MOPD) /cm^{-1}	Windows	Source	Detector	Beamsplitter	Opt. filter /cm^{-1}	Aperture /mm	v^a_{mir} /(cm/s)	Electr. filter /cm^{-1}	No. of scans	Calib. gas [15]
9–45	0.0018	Polyethylene	Hg-Lamp	Si-bolom.	Mylar, 75 μm	0–100	8.0	1.266	39–237	93	H_2O
20–100	0.0018	Polyethylene	Hg-Lamp	Si-bolom.	Mylar, 23 μm	0–100	4.0	1.266	39–237	20	H_2O
90–350	0.0018	Polyethylene	Hg-Lamp	Si-bolom.	Mylar, 6 μm	0–370	2.5	1.266	39–474	75	H_2O

[a] b_{mir}: velocity of the mirror.

a liquid-helium-cooled InSb bolometer. The modulation frequency was 10 kHz and the modulation deviation 250 kHz.

2.3. *Measurements with the high resolution FTIR spectrometer in Gießen*

D_2NCN/DNCND spectra were measured using a Bruker IFS 120 HR Fourier transform interferometer in three overlapping regions from 9 to 350 cm^{-1}, operating with a resolution defined by 1/MOPD (maximum optical path difference) of 0.0018 cm^{-1}. Table 1 gives the chosen instrumental parameters.

The sensitivity of a FTIR spectrometer is considerably less than the sensitivity of a millimetre wave spectrometer. Due to the low vapour pressure of cyanamide (16 Pa at 60°C [11]), we therefore raise the sample and the absorption cell temperatures above room temperature in order to obtain sufficient column density of H_2NCN and HNCNH in the gaseous phase. The increased temperature also shifts the carbodiimide $\rightleftharpoons$ cyanamide equilibrium to the HNCNH side ($p_{(HNCNH)} : p_{(H_2NCN)} = 1 : 115$ at 110°C [12]). During the measurements the cyanamide sample was kept at ≈100°C, and the variable-temperature 3 m absorption cell, developed by Schermaul [16], was maintained at ≈130°C. However, cyanamide decomposes and/or polymerizes quite fast at these temperatures, so that it was necessary to work with a constant mass flow system which led to high sample consumption (≈60 g D_2NCN for the spectra reported here). The D_2NCN spectra will be analysed separately.

3. Spectra, assignment and fits

The NH groups in carbodiimide rotate relative to one another, following a potential function with maxima when the dihedral angle τ between the two hydrogens is either 0° (*cis* conformation) or 180° (*trans* conformation). The *cis* and *trans* maxima of the torsional potential function are nearly of equal height ($V_{cis} = 2061$ and $V_{trans} = 2078$ cm^{-1} [3]). This is due in part to the flexing of the bond angles in HNCNH during the torsional motion. In order to classify the torsional rotational energy levels one can follow the group-theoretical treatment developed by Hougen [17] for H_2X_2 molecules having both a *cis* and *trans* feasible torsional tunnelling. Each rovibrational energy level is split in this case and the resulting levels can be represented by two independent doublet splittings. One doubling of levels results for the *cis* torsional tunnelling and the other doubling for the *trans* torsional tunnelling. The torsional energy levels can be labelled according to the G_4-extended molecular symmetry group [18], with A_{1s}, A_{1d}, A_{2d} and A_{2s}. The lowest energy level belongs to the symmetry species A_{1s} while the uppermost level has the symmetry designation A_{2s}. The relative order of the inner energy levels depends on the relative height of the *cis* and *trans* potential barriers and it was found that the A_{1d} energy level is below the A_{2d} level [1, 2]. The spacing between these two levels is small, because the difference between the *cis* and *trans* potential barriers is small. This is indicated schematically in figure 2.

According to the Pauli principle, the sign of the total wavefunction of the molecule HNCNH must change under the symmetry operation (12) (34), which is the permutation of both the hydrogen and nitrogen nuclei.

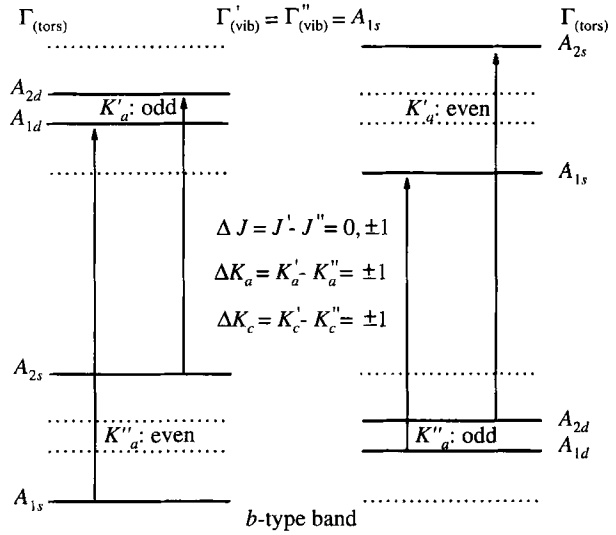

Figure 2. Torsional–rotational selection rules for the vibrational ground state of HNCNH. The levels entered as dotted lines do not exist due to the Pauli principle. The order of the energy levels A_{1d} and A_{2d} implies that $V_{cis} < V_{trans}$.

Table 2. Allowed combinations of symmetry species of the torsional (Γ_{tors}) rotational (Γ_{rot}), and nuclear spin wavefunctions (Γ_{ns}) for HNCNH, $HN^{13}CNH$, $H^{15}NC^{15}NH$, and DNCND in a vibrational state with A_{1s} symmetry.

				Fermions			Bosons			
				HNCNH, $HN^{1}3CNH$			$H^{15}NC^{15}NH$, DNCND			
Γ_{tors}	Γ_{rot}	K_a	K_c	Γ_{ns}	Γ_{tot}	Stat. weight	Γ_{ns}	Γ_{tot}	Stat. weight ^{15}N	Stat. weight D
A_{1s}	A_{1s}	even	even	B_{2s}	B_{2s}	15	A_{1s}	A_{1s}	10	45
A_{1s}	B_{1s}	even	odd	A_{1s}	B_{1s}	21	B_{2s}	A_{2s}	6	36
A_{2s}	A_{1s}	even	even	B_{2s}	B_{1s}	15	A_{1s}	A_{2s}	10	45
A_{2s}	B_{1s}	even	odd	A_{1s}	B_{2s}	21	B_{2s}	A_{1s}	6	36
A_{1d}	A_{2d}	odd	odd	B_{2s}	B_{1s}	15	A_{1s}	A_{2s}	10	45
A_{1d}	B_{2d}	odd	even	A_{1s}	B_{2s}	21	B_{2s}	A_{1s}	6	36
A_{2d}	A_{2d}	odd	odd	B_{2s}	B_{2s}	15	A_{1s}	A_{1s}	10	45
A_{2d}	B_{2d}	odd	even	A_{1s}	B_{1s}	21	B_{2s}	A_{2s}	6	36

The total wavefunction belongs therefore to the irreducible representations denoted by B. Furthermore the sign must not change by an internal rotation of 2π, so that the total wavefunction belongs to the irreducible representations B_{1s} or B_{2s}. This constrains the possible combinations of torsional, rotational, and nuclear spin wavefunctions in a vibrational state with A_{1s} symmetry to those which are given in table 2 [2]. In consequence, for even K_a quantum numbers only the 'outer' torsional energy levels exist, labelled with A_{1s} and A_{2s}, while for odd K_a only the 'inner' energy levels, labelled with A_{1d} and A_{2d}, exist, as displayed in figure 2. We conclude that the torsional motion in carbodiimide leads to a splitting of each rovibrational state into a doublet. According to the rotational state of the molecule, the doublet exhibits either *s* or *d* symmetry.

For HNCNH (and $HN^{13}CNH$) the number of totally symmetric nuclear wavefunctions (A_{1s}) is 21 while the number of antisymmetric wavefunctions (B_{2s}) is 15. The situation changes for $H^{15}NC^{15}NH$ and for DNCND, because the total wavefunction preserves its sign under the symmetry operation (12) (34). This leads to total wavefunctions which belong to the representations labelled with A_{1s} or A_{2s}. For these two isotopomers the allowed combinations of torsional–rotational and nuclear spin wavefunctions in a vibrational state with A_{1s} symmetry are also summarized in table 2. $H^{15}NC^{15}NH$ shows a ratio of symmetric to antisymmetric nuclear wavefunction of 10:6 while this ratio is equal to 45:36 for DNCND. This leads to nuclear spin statistics of 5:3 for $H^{15}NC^{15}NH$ and of 5:4 for DNCND.

The permanent electric dipole moment of carbodiimide coincides with the *b* axis. Therefore a perpendicular *b*-type spectrum, obeying the selection rule $\Delta K_a = +1$, is observed. This means that pure rotational transitions are not allowed for HNCNH, since the torsional state of the molecule must also change when a rotational transition occurs. This is illustrated in figure 2.

The characteristic features of the rotational torsional spectrum are equally spaced Q branches throughout the entire millimetre wave (MMW) and FIR region. The identification of these ${}^rQ_{K_a}$ branches is the key for the assignment of carbodiimide lines in the forest of cyanamide absorptions. The 'aesthetically pleasing' ${}^rQ_0$ branch of the $H^{15}NC^{15}NH$ isotopomer is displayed in figure 3. Due to the torsional motion the branch is doubled, with transitions between $A_{1d} \leftarrow A_{1s}$ and $A_{2d} \leftarrow A_{2s}$ torsional energy levels. The origins of the two Q branches are separated by about 435 MHz. The spin statistics of 5:3 can be seen clearly. Transitions with higher J are shifted to lower frequencies. In this sense the ${}^rQ_0$ branch of $H^{15}NC^{15}NH$ is very similar to that of the main isotopic species [2]. In contrast, a dramatic change occurs in the shape of the ${}^rQ_0$ branch upon going from these isotopomers to the $HN^{13}CNH$ species. This is also shown in figure 3. The ${}^rQ_0$ branch of $HN^{13}CNH$ collapses and the J transitions are only resolved for $J \geqslant 27$. The recorded shape of the strong, unresolved absorption at the subband origin is determined by source modulation with second derivative detection. The torsional splitting is about 455 MHz for $HN^{13}CNH$. A totally different pattern for the ${}^rQ_0$ branch is exhibited by DNCND as is shown in the upper half of figure 4. Due to the deuterium mass, the torsional splitting is reduced by a factor of 100, while the spacing between adjacent J transitions is much larger so that the characteristic compact form of the Q branch is lost. Furthermore the transitions with higher J appear in this case at higher frequencies.

The changes in the shapes of the ${}^rQ_0$ branches described above originate from the near inertial symmetry of the molecule. In this case an explicit expression

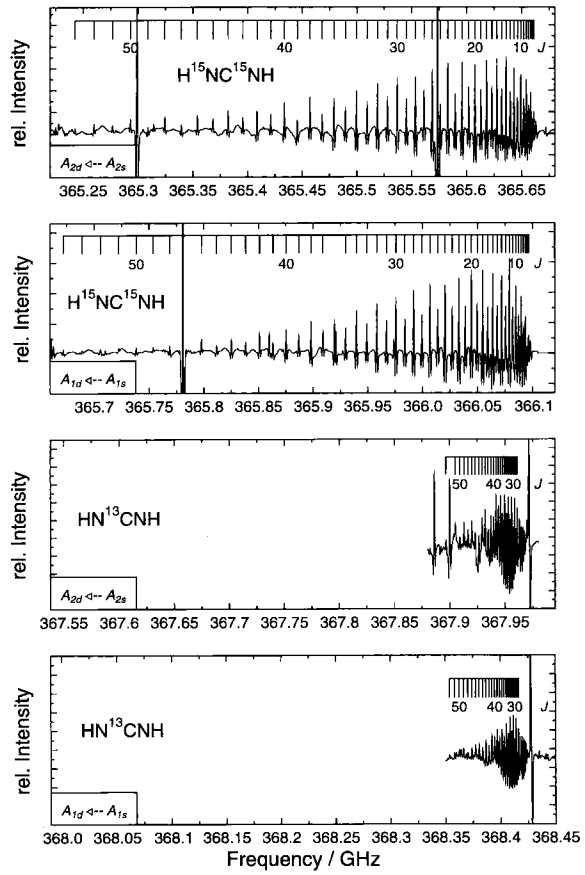

Figure 3. ${}^{r}Q_0$ branches of $H^{15}NC^{15}NH$ and $HN^{13}CNH$. Due to the torsional motion each ${}^{r}Q_0$ branch is doubled. The subbranch at lower frequencies belongs to transitions between $A_{2d} \leftarrow A_{2s}$ torsional energy levels, the subbranch at higher frequencies belongs to transitions between $A_{1d} \leftarrow A_{1s}$ torsional energy levels. The assignment combs indicate the J quantum numbers.

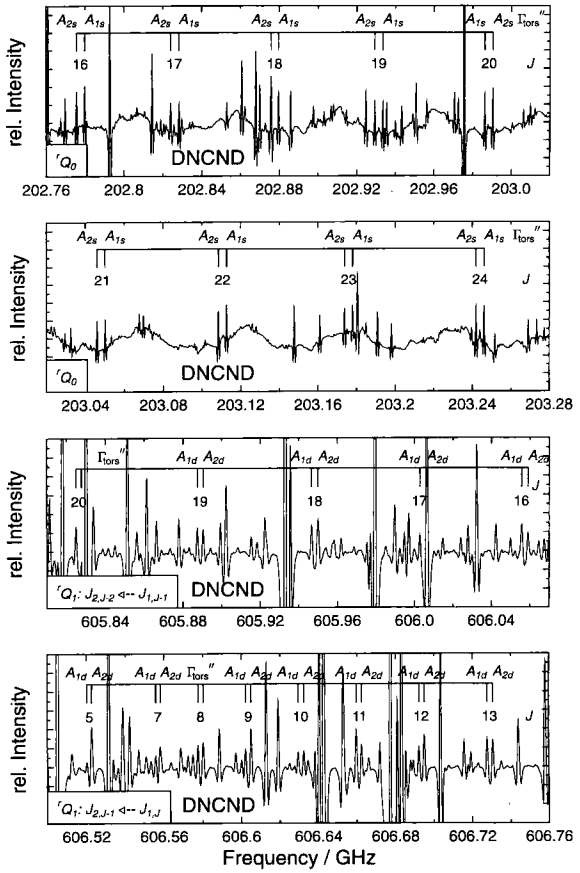

Figure 4. Part of the ${}^{r}Q_0$ and ${}^{r}Q_1$ branches of DNCND. Compared with the other carbodiimide isotopomers the torsional splitting is decreased by a factor of 100. The two components of the torsional doublet are labelled with the symmetry species $\Gamma'' \in \{A_{1s}, A_{2s}\}$ of the lower torsional energy level. The J assignment is indicated.

for frequencies ν of the ${}^{r}Q_0$ branch lines can be given [19]:

$$\nu \approx \left[A - \tfrac{1}{2}(B+C) - D_K\right] + \left[\tfrac{1}{4}(B-C) - D_{JK}\right] \times J(J+1) + \cdots . \quad (1)$$

where A, B, and C are the rotational constants, and D_K and D_{JK} are quartic centrifugal distortion constants.

In the case of $H^{15}NC^{15}NH$, which is the the most inertially symmetric species of the investigated HNCNH isotopomers, the difference between the rotational constants B and C is so small that the $J(J+1)$ dependent term is dominated by the negative contribution of the large centrifugal distortion constant D_{JK}. For the $HN^{13}CNH$ species the two contributions are nearly equal causing the unusually condensed appearance of the observed Q branch. For DNCND, however, which is the most asymmetric isotopomer, the pattern of the ${}^{r}Q_0$ branch is dominated by the inertial asymmetry contribution. The centrifugal distortion constant D_{JK} of DNCND is an order of magnitude smaller than for the other isotopomers (see below).

The J assignments of the Q branches were performed by using an interactive assignment program QBRASS [20], where the transition frequencies belonging to a particular subbranch were fitted to a power series (ps) expression in $J(J+1)$:

$$\nu = \nu_c + \Delta B_{ps} J(J+1) - \Delta D_{ps} J^2 (J+1)^2 . \quad (2)$$

The criteria supporting the correct assignment were the minimal standard deviation together with the information drawn from the nuclear spin statistics. The assignments were then confirmed in each case by measuring ${}^{r}P_0$- and ${}^{p}R_1$-branch transitions in the MMW region, which could be identified among the cyanamide absorptions after the Q branches had been found. All measured transitions of the isotopomers $H^{15}NC^{15}NH$ and

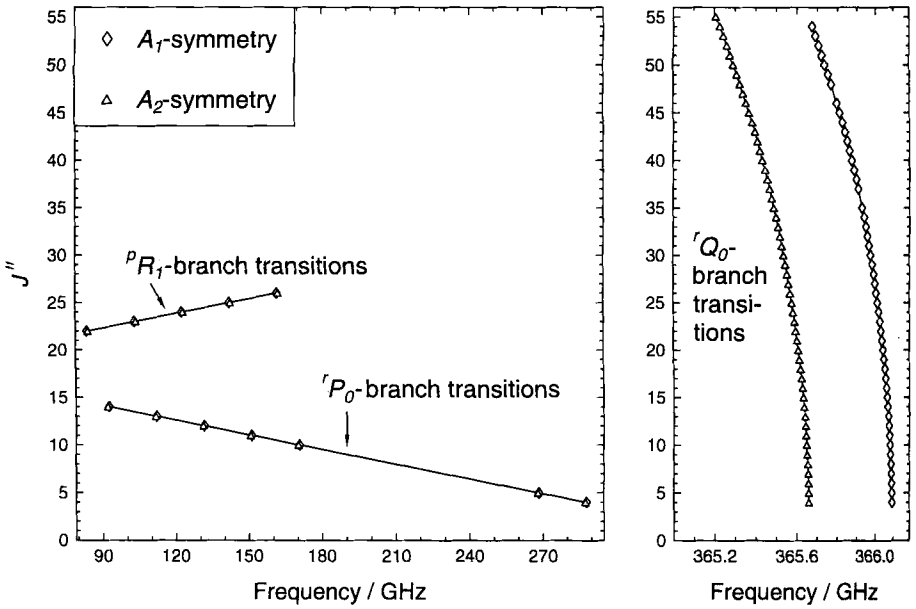

Figure 5. Fortrat diagrams of all measured $H^{15}NC^{15}NH$ transitions.

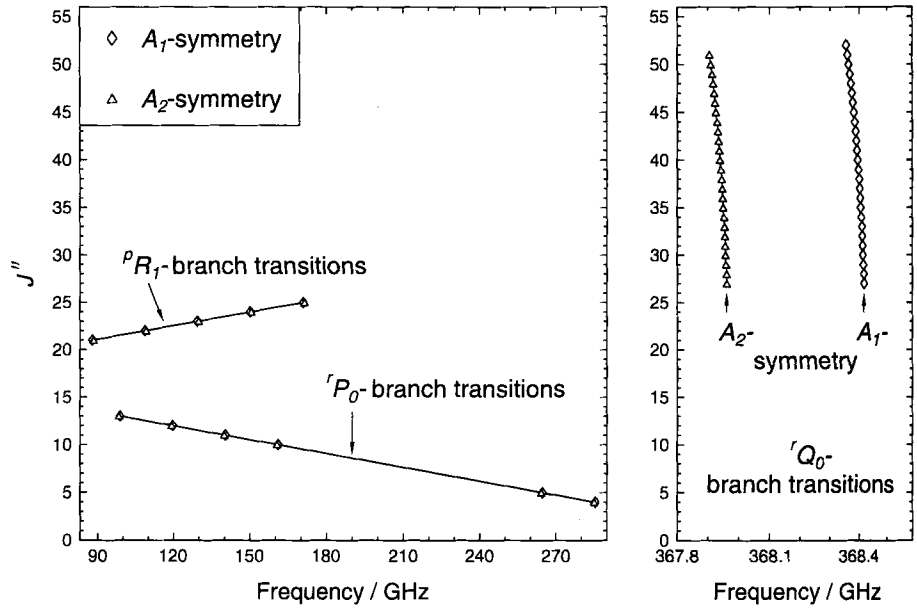

Figure 6. Fortrat diagrams of all measured $HN^{13}CNH$ transitions.

$HN^{13}CNH$ are graphically presented in the Fortrat diagrams of figures 5 and 6, and the transition frequencies are listed in tables 3 and 4. Due to the overlapping of strong D_2NCN lines only two $^pR_1$-branch transitions could be measured for DNCND. However, additional information was gained by assigning many $^rQ_1$-branch transitions at 606.5 GHz. Parts of this branch are shown in the lower half of figure 4. This branch consists of four subbranches, due to the K_a doubling and the torsional doubling of the energy levels. The serious overlap with D_2NCN lines is obvious and prevented following the series of transitions to high J values. The Fortrat diagrams of the DNCND $^rQ_0$ and $^rQ_1$ branch transitions are given in figure 7. The transition frequencies are presented in table 5.

As mentioned above, the FIR spectrum of DNCND was recorded. The nearly equally spaced $^rQ_{K_a}$ branches were followed up to $K_a = 10$. They are displayed in figure 8. A plot of the subband centres versus $2K_a + 1$ is shown in figure 9. The almost linear relationship is

Table 3. Assigned transitions of $H^{15}NC^{15}NH$ together with the centre frequencies of each torsional doublet. The centre frequencies were fitted to the Watson Hamiltonian in *S* reduction. The differences between the centre frequencies and those calculated with the constants of table 7 are also listed.

$J'_{K'_a,K'_c} \leftarrow J''_{K''_a,K''_c}$	$\Gamma'_{tors} \leftarrow \Gamma''_{tors}$	Measured transitions/MHz	Centre frequency /MHz	$\nu_{cent} - \nu_{calc.}$/MHz
$^rQ_0$-branch transitions				
$4_{1,3} \leftarrow 4_{0,4}$	$A_{1d} \leftarrow A_{1s}$ $A_{2d} \leftarrow A_{2s}$	366 096.214 365 661.037	365 878.626	0.0167
$5_{1,4} \leftarrow 5_{0,5}$	$A_{1d} \leftarrow A_{1s}$ $A_{2d} \leftarrow A_{2s}$	366 094.905 365 659.693	365 877.299	−0.0175
$6_{1,5} \leftarrow 6_{0,6}$	$A_{1d} \leftarrow A_{1s}$ $A_{2d} \leftarrow A_{2s}$	366 093.373 365 658.127	365 875.750	−0.0136
$7_{1,6} \leftarrow 7_{0,7}$	$A_{1d} \leftarrow A_{1s}$ $A_{2d} \leftarrow A_{2s}$	366 091.582 365 656.285	365 873.934	−0.0159
$8_{1,7} \leftarrow 8_{0,8}$	$A_{1d} \leftarrow A_{1s}$ $A_{2d} \leftarrow A_{2s}$	366 089.555 365 654.179	365 871.867	−0.0074
$9_{1,8} \leftarrow 9_{0.9}$	$A_{1d} \leftarrow A_{1s}$ $A_{2d} \leftarrow A_{2s}$	366 087.256 365 651.800	365 869.528	−0.0079
$10_{1,9} \leftarrow 10_{0,10}$	$A_{1d} \leftarrow A_{1s}$ $A_{2d} \leftarrow A_{2s}$	366 084.755 365 649.164	365 866.959	0.0256
$11_{1,10} \leftarrow 11_{0,11}$	$A_{1d} \leftarrow A_{1s}$ $A_{2d} \leftarrow A_{2s}$	366 081.873 365 646.246	365 864.059	−0.0064
$12_{1,11} \leftarrow 12_{0,12}$	$A_{1d} \leftarrow A_{1s}$ $A_{2d} \leftarrow A_{2s}$	366 078.847 365 643.066	365 860.956	0.0255
$13_{1,12} \leftarrow 13_{0,13}$	$A_{1d} \leftarrow A_{1s}$ $A_{2d} \leftarrow A_{2s}$	366 075.436 365 639.615	365 857.525	−0.0020
$14_{1,13} \leftarrow 14_{0,14}$	$A_{1d} \leftarrow A_{1s}$ $A_{2d} \leftarrow A_{2s}$	366 071.818 365 635.887	365 853.853	−0.0002
$15_{1,14} \leftarrow 15_{0,15}$	$A_{1d} \leftarrow A_{1s}$ $A_{2d} \leftarrow A_{2s}$	366 067.930 365 631.884	365 849.907	−0.0002
$16_{1,15} \leftarrow 16_{0,16}$	$A_{1d} \leftarrow A_{1s}$ $A_{2d} \leftarrow A_{2s}$	366 063.781 365 627.592	365 845.687	0.0001
$17_{1,16} \leftarrow 17_{0,17}$	$A_{1d} \leftarrow A_{1s}$ $A_{2d} \leftarrow A_{2s}$	366 059.355 365 623.024	365 841.189	−0.0013
$18_{1,17} \leftarrow 18_{0,18}$	$A_{1d} \leftarrow A_{1s}$ $A_{2d} \leftarrow A_{2s}$	366 054.656 365 618.173	365 836.415	0.0000
$19_{1,18} \leftarrow 19_{0,19}$	$A_{1d} \leftarrow A_{1s}$ $A_{2d} \leftarrow A_{2s}$	366 049.676 365 613.040	365 831.358	−0.0005
$20_{1,19} \leftarrow 20_{0,20}$	$A_{1d} \leftarrow A_{1s}$ $A_{2d} \leftarrow A_{2s}$	366 044.415 365 607.620	365 826.018	−0.0003
$21_{1,20} \leftarrow 21_{0,21}$	$A_{1d} \leftarrow A_{1s}$ $A_{2d} \leftarrow A_{2s}$	366 038.877 365 601.911	365 820.394	0.0022
$22_{1,21} \leftarrow 22_{0,22}$	$A_{1d} \leftarrow A_{1s}$ $A_{2d} \leftarrow A_{2s}$	366 033.043 365 595.906	365 814.475	−0.0010
$23_{1,22} \leftarrow 23_{0,23}$	$A_{1d} \leftarrow A_{1s}$ $A_{2d} \leftarrow A_{2s}$	366 026.936 365 589.603	365 808.269	0.0010

(*continued*)

Table 3 (*continued*)

$J'_{K'_a,K'_c} \leftarrow J''_{K''_a,K''_c}$	$\Gamma'_{\text{tors}} \leftarrow \Gamma''_{\text{tors}}$	Measured transitions/MHz	Centre frequency /MHz	$\nu_{\text{cent}} - \nu_{\text{calc.}}$/MHz
$24_{1,23} \leftarrow 24_{0,24}$	$A_{1d} \leftarrow A_{1s}$ $A_{2d} \leftarrow A_{2s}$	366 020.531 365 582.999	365 801.765	0.0003
$25_{1,24} \leftarrow 25_{0,25}$	$A_{1d} \leftarrow A_{1s}$ $A_{2d} \leftarrow A_{2s}$	366 013.834 365 576.131	365 794.982	0.0191
$26_{1,25} \leftarrow 26_{0,26}$	$A_{1d} \leftarrow A_{1s}$ $A_{2d} \leftarrow A_{2s}$	366 006.831 365 568.887	365 787.859	−0.0001
$27_{1,26} \leftarrow 27_{0,27}$	$A_{1d} \leftarrow A_{1s}$ $A_{2d} \leftarrow A_{2s}$	365 999.529 365 561.373	365 780.451	0.0011
$28_{1,27} \leftarrow 28_{0,28}$	$A_{1d} \leftarrow A_{1s}$ $A_{2d} \leftarrow A_{2s}$	365 991.922 365 553.535	365 772.728	−0.0035
$29_{1,28} \leftarrow 29_{0,29}$	$A_{1d} \leftarrow A_{1s}$ $A_{2d} \leftarrow A_{2s}$	365 984.009 365 545.387	365 764.698	−0.0024
$30_{1,29} \leftarrow 30_{0,30}$	$A_{1d} \leftarrow A_{1s}$ $A_{2d} \leftarrow A_{2s}$	365 975.791 365 536.925	365 756.358	0.0056
$31_{1,30} \leftarrow 31_{0,31}$	$A_{1d} \leftarrow A_{1s}$ $A_{2d} \leftarrow A_{2s}$	365 967.232 365 528.132	365 747.682	−0.0015
$32_{1,31} \leftarrow 32_{0,32}$	$A_{1d} \leftarrow A_{1s}$ $A_{2d} \leftarrow A_{2s}$	365 958.372 365 518.997	365 738.684	−0.0057
$33_{1,32} \leftarrow 33_{0,33}$	$A_{1d} \leftarrow A_{1s}$ $A_{2d} \leftarrow A_{2s}$	365 949.186 365 509.546	365 729.366	−0.0004
$34_{1,33} \leftarrow 34_{0,34}$	$A_{1d} \leftarrow A_{1s}$ $A_{2d} \leftarrow A_{2s}$	365 939.665 365 499.754	365 719.709	−0.0004
$35_{1,34} \leftarrow 35_{0,35}$	$A_{1d} \leftarrow A_{1s}$ $A_{2d} \leftarrow A_{2s}$	365 929.812 365 489.616	365 709.714	0.0001
$37_{1,36} \leftarrow 37_{0,37}$	$A_{1d} \leftarrow A_{1s}$ $A_{2d} \leftarrow A_{2s}$	365 909.078 365 468.290	365 688.684	−0.0047
$38_{1,37} \leftarrow 38_{0,38}$	$A_{1d} \leftarrow A_{1s}$ $A_{2d} \leftarrow A_{2s}$	365 898.189 365 457.107	365 677.648	−0.0011
$39_{1,38} \leftarrow 39_{0,39}$	$A_{1d} \leftarrow A_{1s}$ $A_{2d} \leftarrow A_{2s}$	365 886.942 365 445.559	365 666.250	−0.0013
$40_{1,39} \leftarrow 40_{0,40}$	$A_{1d} \leftarrow A_{1s}$ $A_{2d} \leftarrow A_{2s}$	365 875.359 365 433.647	365 654.503	0.0129
$41_{1,40} \leftarrow 41_{0,41}$	$A_{1d} \leftarrow A_{1s}$ $A_{2d} \leftarrow A_{2s}$	365 863.374 365 421.339	365 642.356	−0.0041
$42_{1,41} \leftarrow 42_{0,42}$	$A_{1d} \leftarrow A_{1s}$ $A_{2d} \leftarrow A_{2s}$	365 851.054 365 408.668	365 629.861	0.0052
$43_{1,42} \leftarrow 43_{0,43}$	$A_{1d} \leftarrow A_{1s}$ $A_{2d} \leftarrow A_{2s}$	365 838.324 365 395.615	365 616.970	−0.0014
$44_{1,43} \leftarrow 44_{0,44}$	$A_{1d} \leftarrow A_{1s}$ $A_{2d} \leftarrow A_{2s}$	365 825.236 365 382.160	365 603.698	−0.0032
$45_{1,44} \leftarrow 45_{0,45}$	$A_{1d} \leftarrow A_{1s}$ $A_{2d} \leftarrow A_{2s}$	365 811.764 365 368.320	365 590.042	0.0029
$46_{1,45} \leftarrow 46_{0,46}$	$A_{1d} \leftarrow A_{1s}$ $A_{2d} \leftarrow A_{2s}$	365 797.871 365 354.075	365 575.973	−0.0062

Table 3 (*continued*)

$J'_{K'_a,K'_c} \leftarrow J''_{K''_a,K''_c}$	$\Gamma'_{\text{tors}} \leftarrow \Gamma''_{\text{tors}}$	Measured transition/MHz	Centre frequency /MHz	$\nu_{\text{cent}} - \nu_{\text{calc.}}$/MHz
$48_{1,47} \leftarrow 48_{0,48}$	$A_{1d} \leftarrow A_{1s}$	365 768.899	365 546.630	−0.0107
	$A_{2d} \leftarrow A_{2s}$	365 324.362		
$49_{1,48} \leftarrow 49_{0,49}$	$A_{1d} \leftarrow A_{1s}$	365 753.815	365 531.359	0.0097
	$A_{2d} \leftarrow A_{2s}$	365 308.903		
$50_{1,49} \leftarrow 50_{0,50}$	$A_{1d} \leftarrow A_{1s}$	365 738.297	365 515.634	−0.0003
	$A_{2d} \leftarrow A_{2s}$	365 292.970		
$51_{1,50} \leftarrow 51_{0,51}$	$A_{1d} \leftarrow A_{1s}$	365 722.398	365 499.514	0.0250
	$A_{2d} \leftarrow A_{2s}$	365 276.630		
$52_{1,51} \leftarrow 52_{0,52}$	$A_{1d} \leftarrow A_{1s}$	365 705.805	365 482.836	−0.0704
	$A_{2d} \leftarrow A_{2s}$	365 259.867		
$53_{1,52} \leftarrow 53_{0,53}$	$A_{1d} \leftarrow A_{1s}$	365 689.175	365 465.881	0.0014
	$A_{2d} \leftarrow A_{2s}$	365 242.587		
$54_{1,53} \leftarrow 54_{0,54}$	$A_{1d} \leftarrow A_{1s}$	365 671.927	365 448.442	0.0406
	$A_{2d} \leftarrow A_{2s}$	365 224.956		
$^rP_0$-branch transitions				
$3_{1,3} \leftarrow 4_{0,4}$	$A_{1d} \leftarrow A_{1s}$	287 920.869	287 703.419	−0.0023
	$A_{2d} \leftarrow A_{2s}$	287 485.969		
$4_{1,4} \leftarrow 5_{0,5}$	$A_{1d} \leftarrow A_{1s}$	268 374.353	268 156.976	−0.0068
	$A_{2d} \leftarrow A_{2s}$	267 939.600		
$9_{1,9} \leftarrow 10_{0,10}$	$A_{1d} \leftarrow A_{1s}$	170 633.187	170 416.304	0.0007
	$A_{2d} \leftarrow A_{2s}$	170 199.421		
$11_{1,11} \leftarrow 12_{0,12}$	$A_{1d} \leftarrow A_{1s}$	131 533.999	131 317.396	0.0153
	$A_{2d} \leftarrow A_{2s}$	131 100.793		
$12_{1,12} \leftarrow 13_{0,13}$	$A_{1d} \leftarrow A_{1s}$	111 984.067	111 767.624	−0.0093
	$A_{2d} \leftarrow A_{2s}$	111 551.180		
$13_{1,13} \leftarrow 14_{0,14}$	$A_{1d} \leftarrow A_{1s}$	92 434.067	92 217.791	0.0015
	$A_{2d} \leftarrow A_{2s}$	92 001.515		
$^pR_1$-branch transitions				
$23_{0,23} \leftarrow 22_{1,22}$	$A_{1d} \leftarrow A_{1s}$	83 509.214	83 723.391	0.0039
	$A_{2d} \leftarrow A_{2s}$	83 937.567		
$24_{0,24} \leftarrow 23_{1,23}$	$A_{1d} \leftarrow A_{1s}$	103 056.388	103 270.272	0.0029
	$A_{2d} \leftarrow A_{2s}$	103 484.156		
$25_{0,25} \leftarrow 24_{1,24}$	$A_{1d} \leftarrow A_{1s}$	122 602.901	122 816.459	−0.0005
	$A_{2d} \leftarrow A_{2s}$	123 030.017		
$26_{0,26} \leftarrow 25_{1,25}$	$A_{1d} \leftarrow A_{1s}$	142 148.617	142 361.884	−0.0017
	$A_{2d} \leftarrow A_{2s}$	142 575.150		
$27_{0,27} \leftarrow 26_{1.26}$	$A_{1d} \leftarrow A_{1s}$	161 693.541	161 906.473	−0.0021
	$A_{2d} \leftarrow A_{2s}$	162 119.404		

indeed expected for an unperturbed perpendicular band system. The Q branches are rotationally resolved only for $K_a \geqslant 9$, while this is true for $K_a \geqslant 4$ in the case of the main species. This is caused by a centrifugal distortion constant D_{JK} which is an order of magnitude smaller for DNCND than for the main species (see below) [1].

After the identification of the Q branches, the transitions belonging to $^rR_{K_a}$ branches were also found and assigned with the aid of a Loomis–Wood program [20].

Table 4. Assigned transitions of $HN^{13}CNH$ together with the centre frequencies of each torsional doublet. The centre frequencies were fitted to the Watson Hamiltonian in *S* reduction. The differences between the centre frequencies and those calculated with the constants of table 7 are also listed.

$J'_{K'_a,K'_c} \leftarrow J''_{K''_a,K''_c}$	$\Gamma'_{tors} \leftarrow \Gamma''_{tors}$	Measured transitions/MHz	Centre frequency /MHz	$\nu_{cent} - \nu_{calc.}$/MHz
$^rQ_0$-branch transitions				
$27_{1,26} \leftarrow 27_{0,27}$	$A_{1d} \leftarrow A_{1s}$ $A_{2d} \leftarrow A_{2s}$	368 416.539 367 960.850	368 188.695	0.0129
$28_{1,27} \leftarrow 28_{0,28}$	$A_{1d} \leftarrow A_{1s}$ $A_{2d} \leftarrow A_{2s}$	368 415.422 367 959.767	368 187.595	0.0150
$29_{1,28} \leftarrow 29_{0,29}$	$A_{1d} \leftarrow A_{1s}$ $A_{2d} \leftarrow A_{2s}$	368 414.230 367 958.568	368 186.399	−0.0024
$30_{1,29} \leftarrow 30_{0,30}$	$A_{1d} \leftarrow A_{1s}$ $A_{2d} \leftarrow A_{2s}$	368 412.967 367 957.311	368 185.139	−0.0032
$31_{1,30} \leftarrow 31_{0,31}$	$A_{1d} \leftarrow A_{1s}$ $A_{2d} \leftarrow A_{2s}$	368 411.625 367 955.975	368 183.800	0.0016
$32_{1,31} \leftarrow 32_{0,32}$	$A_{1d} \leftarrow A_{1s}$ $A_{2d} \leftarrow A_{2s}$	368 410.166 367 954.546	368 182.356	−0.0098
$33_{1,32} \leftarrow 33_{0,33}$	$A_{1d} \leftarrow A_{1s}$ $A_{2d} \leftarrow A_{2s}$	368 408.634 367 953.035	368 180.835	−0.0051
$34_{1,33} \leftarrow 34_{0,34}$	$A_{1d} \leftarrow A_{1s}$ $A_{2d} \leftarrow A_{2s}$	368 406.993 367 951.433	368 179.213	−0.0039
$35_{1,34} \leftarrow 35_{0,35}$	$A_{1d} \leftarrow A_{1s}$ $A_{2d} \leftarrow A_{2s}$	368 405.244 367 949.733	368 177.489	−0.0024
$36_{1,35} \leftarrow 36_{0,36}$	$A_{1d} \leftarrow A_{1s}$ $A_{2d} \leftarrow A_{2s}$	368 403.389 367 947.924	368 175.657	−0.0021
$37_{1,36} \leftarrow 37_{0,37}$	$A_{1d} \leftarrow A_{1s}$ $A_{2d} \leftarrow A_{2s}$	368 401.401 367 946.017	368 173.709	−0.0060
$38_{1,37} \leftarrow 38_{0,38}$	$A_{1d} \leftarrow A_{1s}$ $A_{2d} \leftarrow A_{2s}$	368 399.292 367 943.988	368 171.640	−0.0141
$39_{1,38} \leftarrow 39_{0,39}$	$A_{1d} \leftarrow A_{1s}$ $A_{2d} \leftarrow A_{2s}$	368 397.081 367 941.863	368 169.472	0.0008
$40_{1,39} \leftarrow 40_{0,40}$	$A_{1d} \leftarrow A_{1s}$ $A_{2d} \leftarrow A_{2s}$	368 394.724 367 939.615	368 167.170	0.0088
$41_{1,40} \leftarrow 41_{0,41}$	$A_{1d} \leftarrow A_{1s}$ $A_{2d} \leftarrow A_{2s}$	368 392.222 367 937.215	368 164.719	0.0004
$42_{1,41} \leftarrow 42_{0,42}$	$A_{1d} \leftarrow A_{1s}$ $A_{2d} \leftarrow A_{2s}$	368 389.574 367 934.684	368 162.129	−0.0088
$43_{1,42} \leftarrow 43_{0,43}$	$A_{1d} \leftarrow A_{1s}$ $A_{2d} \leftarrow A_{2s}$	368 386.815 367 932.017	368 159.416	0.0028
$44_{1,43} \leftarrow 44_{0,44}$	$A_{1d} \leftarrow A_{1s}$ $A_{2d} \leftarrow A_{2s}$	368 383.817 367 929.274	368 156.546	0.0071
$45_{1,44} \leftarrow 45_{0,45}$	$A_{1d} \leftarrow A_{1s}$ $A_{2d} \leftarrow A_{2s}$	368 380.724 367 926.331	368 153.528	0.0190
$47_{1,46} \leftarrow 47_{0,47}$	$A_{1d} \leftarrow A_{1s}$ $A_{2d} \leftarrow A_{2s}$	368 374.001 367 919.942	368 146.972	0.0140
$48_{1,47} \leftarrow 48_{0,48}$	$A_{1d} \leftarrow A_{1s}$ $A_{2d} \leftarrow A_{2s}$	368 370.364 367 916.452	368 143.408	−0.0162

Table 4 (*continued*)

$J'_{K'_a,K'_c} \leftarrow J''_{K''_a,K''_c}$	$\Gamma'_{\text{tors}} \leftarrow \Gamma''_{\text{tors}}$	Measured transitions/MHz	Centre frequency /MHz	$\nu_{\text{cent}} - \nu_{\text{calc.}}$/MHz
$49_{1,48} \leftarrow 49_{0,49}$	$A_{1d} \leftarrow A_{1s}$	368 366.506	368 139.696	−0.0137
	$A_{2d} \leftarrow A_{2s}$	367 912.885		
$50_{1,49} \leftarrow 50_{0,50}$	$A_{1d} \leftarrow A_{1s}$	368 362.537	368 135.831	0.0233
	$A_{2d} \leftarrow A_{2s}$	367 909.124		
$51_{1,50} \leftarrow 51_{0,51}$	$A_{1d} \leftarrow A_{1s}$	368 358.272	368 131.696	−0.0156
	$A_{2d} \leftarrow A_{2s}$	367 905.119		
$^rP_0$-branch transitions				
$3_{1,2} \leftarrow 4_{0,4}$	$A_{1d} \leftarrow A_{1s}$	285 487.205	285 259.310	0.0045
	$A_{2d} \leftarrow A_{2s}$	285 031.414		
$4_{1,4} \leftarrow 5_{0,5}$	$A_{1d} \leftarrow A_{1s}$	264 749.249	264 521.491	−0.0130
	$A_{2d} \leftarrow A_{2s}$	264 293.733		
$11_{1,11} \leftarrow 12_{0,12}$	$A_{1d} \leftarrow A_{1s}$	119 563.478	119 336.541	0.0127
	$A_{2d} \leftarrow A_{2s}$	119 109.604		
$12_{1,12} \leftarrow 13_{0,13}$	$A_{1d} \leftarrow A_{1s}$	98 820.604	98 593.852	−0.0032
	$A_{2d} \leftarrow A_{2s}$	98 367.099		
$^pR_1$-branch transitions				
$22_{0,22} \leftarrow 21_{1,21}$	$A_{1d} \leftarrow A_{1s}$	87 867.496	88 092.009	0.0090
	$A_{2d} \leftarrow A_{2s}$	88 316.522		
$23_{0,23} \leftarrow 22_{1,22}$	$A_{1d} \leftarrow A_{1s}$	108 609.407	108 833.604	0.0011
	$A_{2d} \leftarrow A_{2s}$	109 057.802		
$24_{0,24} \leftarrow 23_{1,23}$	$A_{1d} \leftarrow A_{1s}$	129 350.763	129 574.651	−0.0053
	$A_{2d} \leftarrow A_{2s}$	129 798.539		
$25_{0,25} \leftarrow 24_{1,24}$	$A_{1d} \leftarrow A_{1s}$	150 091.563	150 315.080	0.0007
	$A_{2d} \leftarrow A_{2s}$	150 538.597		
$26_{0,26} \leftarrow 25_{1,25}$	$A_{1d} \leftarrow A_{1s}$	170 831.626	170 054.789	−0.0018
	$A_{2d} \leftarrow A_{2s}$	171 277.952		

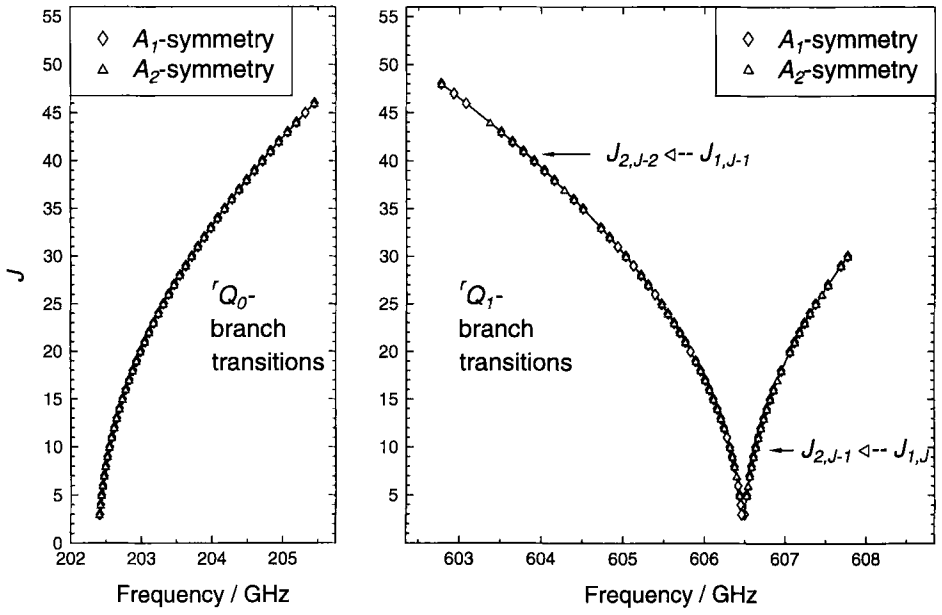

Figure 7. Fortrat diagrams of the measured DNCND Q-branch transitions in the MMW region. Due to the decreased torsional splitting and the higher asymmetry of DNCND compared with the other isotopomers, the torsional splitting is not resolved.

Table 5. Assigned transitions of DNCND in the MMW and SubMMW region. The centre frequencies of the torsional doublets were fitted to the Watson Hamiltonian in *S* reduction together with the observed IR transition wavenumbers given in table 6. The differences between the centre frequencies and those calculated with the constants of table 7 are also listed.

$J'_{K'_a,K'_c} \leftarrow J''_{K''_a,K''_c}$	$\Gamma'_{\text{tors}} \leftarrow \Gamma''_{\text{tors}}$	Measured transition/MHz	Centre frequency/MHz	$\nu_{\text{cent}} - \nu_{\text{calc.}}$/MHz
$^rQ_0$-branch transitions				
$3_{1,2} \leftarrow 3_{0,3}$	$A_{1d} \leftarrow A_{1s}$	202 409.184	202 407.127	0.0645
	$A_{2d} \leftarrow A_{2s}$	202 405.070		
$4_{1,3} \leftarrow 4_{0,4}$	$A_{1d} \leftarrow A_{1s}$	202 420.608	202 418.508	0.0260
	$A_{2d} \leftarrow A_{2s}$	202 416.409		
$5_{1,4} \leftarrow 5_{0,5}$	$A_{1d} \leftarrow A_{1s}$	202 434.526	202 432.637	−0.1180
	$A_{2d} \leftarrow A_{2s}$	202 430.748		
$6_{1,5} \leftarrow 6_{0,6}$	$A_{1d} \leftarrow A_{1s}$	202 451.984	202 449.936	0.0550
	$A_{2d} \leftarrow A_{2s}$	202 447.889		
$7_{1,6} \leftarrow 7_{0,7}$	$A_{1d} \leftarrow A_{1s}$	202 471.634	202 469.742	−0.1170
	$A_{2d} \leftarrow A_{2s}$	202 467.850		
$8_{1,7} \leftarrow 8_{0,8}$	$A_{1d} \leftarrow A_{1s}$	202 494.810	202 492.741	0.0539
	$A_{2d} \leftarrow A_{2s}$	202 490.672		
$9_{1,8} \leftarrow 9_{0,9}$	$A_{1d} \leftarrow A_{1s}$	202 520.474	202 518.384	0.0192
	$A_{2d} \leftarrow A_{2s}$	202 516.295		
$10_{1,9} \leftarrow 10_{0,10}$	$A_{1d} \leftarrow A_{1s}$	202 549.005	202 546.887	−0.0034
	$A_{2d} \leftarrow A_{2s}$	202 544.769		
$11_{1,10} \leftarrow 11_{0,11}$	$A_{1d} \leftarrow A_{1s}$	202 580.382	202 578.270	0.0078
	$A_{2d} \leftarrow A_{2s}$	202 576.159		
$12_{1,11} \leftarrow 12_{0,12}$	$A_{1d} \leftarrow A_{1s}$	202 614.612	202 612.529	0.0506
	$A_{2d} \leftarrow A_{2s}$	202 610.447		
$13_{1,12} \leftarrow 13_{0,13}$	$A_{1d} \leftarrow A_{1s}$	202 651.656	202 649.580	0.0430
	$A_{2d} \leftarrow A_{2s}$	202 647.505		
$14_{1,13} \leftarrow 14_{0,14}$	$A_{1d} \leftarrow A_{1s}$	202 691.557	202 689.475	0.0391
	$A_{2d} \leftarrow A_{2s}$	202 687.392		
$15_{1,14} \leftarrow 15_{0,15}$	$A_{1d} \leftarrow A_{1s}$	202 734.293	202 732.212	0.0393
	$A_{2d} \leftarrow A_{2s}$	202 730.131		
$16_{1,15} \leftarrow 16_{0,16}$	$A_{1d} \leftarrow A_{1s}$	202 779.860	202 777.787	0.0421
	$A_{2d} \leftarrow A_{2s}$	202 775.713		
$17_{1,16} \leftarrow 17_{0,17}$	$A_{1d} \leftarrow A_{1s}$	202 828.275	202 826.140	−0.0100
	$A_{2d} \leftarrow A_{2s}$	202 824.005		
$19_{1,18} \leftarrow 19_{0,19}$	$A_{1d} \leftarrow A_{1s}$	202 933.571	202 931.483	0.0357
	$A_{2d} \leftarrow A_{2s}$	202 929.395		
$20_{1,19} \leftarrow 20_{0,20}$	$A_{1d} \leftarrow A_{1s}$	202 990.460	202 988.362	0.0287
	$A_{2d} \leftarrow A_{2s}$	202 986.265		
$21_{1,20} \leftarrow 21_{0,21}$	$A_{1d} \leftarrow A_{1s}$	203 050.160	203 048.064	0.0241
	$A_{2d} \leftarrow A_{2s}$	203 045.967		
$22_{1,21} \leftarrow 22_{0,22}$	$A_{1d} \leftarrow A_{1s}$	203 112.682	203 110.579	0.0154
	$A_{2d} \leftarrow A_{2s}$	203 108.475		
$23_{1,22} \leftarrow 23_{0,23}$	$A_{1d} \leftarrow A_{1s}$	203 178.045	203 175.921	0.0202
	$A_{2d} \leftarrow A_{2s}$	203 173.797		
$24_{1,23} \leftarrow 24_{0,24}$	$A_{1d} \leftarrow A_{1s}$	203 246.184	203 244.074	0.0264
	$A_{2d} \leftarrow A_{2s}$	203 241.964		
$25_{1,24} \leftarrow 25_{0,25}$	$A_{1d} \leftarrow A_{1s}$	203 317.132	203 315.014	0.0140
	$A_{2d} \leftarrow A_{2s}$	203 312.895		

Table 5 (*continued*)

$J'_{K'_a,K'_c} \leftarrow J''_{K''_a,K''_c}$	$\Gamma'_{\text{tors}} \leftarrow \Gamma''_{\text{tors}}$	Measured transition/MHz	Centre frequency/MHz	$\nu_{\text{cent}} - \nu_{\text{calc.}}$/MHz
$26_{1,25} \leftarrow 26_{0,26}$	$A_{1d} \leftarrow A_{1s}$ $A_{2d} \leftarrow A_{2s}$	203 390.836 203 386.628	203 388.732	−0.0220
$27_{1,26} \leftarrow 27_{0,27}$	$A_{1d} \leftarrow A_{1s}$ $A_{2d} \leftarrow A_{2s}$	203 467.455 203 463.178	203 465.317	0.0118
$28_{1,27} \leftarrow 28_{0,28}$	$A_{1d} \leftarrow A_{1s}$ $A_{2d} \leftarrow A_{2s}$	203 546.774 203 542.505	203 544.640	−0.0091
$29_{1,28} \leftarrow 29_{0,29}$	$A_{1d} \leftarrow A_{1s}$ $A_{2d} \leftarrow A_{2s}$	203 628.895 203 624.658	203 626.777	−0.0040
$30_{1,29} \leftarrow 30_{0,30}$	$A_{1d} \leftarrow A_{1s}$ $A_{2d} \leftarrow A_{2s}$	203 713.832 203 709.531	203 711.682	−0.0141
$31_{1,30} \leftarrow 31_{0,31}$	$A_{1d} \leftarrow A_{1s}$ $A_{2d} \leftarrow A_{2s}$	203 801.534 203 797.229	203 799.381	−0.0085
$32_{1,31} \leftarrow 32_{0,32}$	$A_{1d} \leftarrow A_{1s}$ $A_{2d} \leftarrow A_{2s}$	203 892.019 203 887.690	203 889.855	−0.0010
$33_{1,32} \leftarrow 33_{0,33}$	$A_{1d} \leftarrow A_{1s}$ $A_{2d} \leftarrow A_{2s}$	203 985.232 203 980.907	203 983.070	−0.0202
$34_{1,33} \leftarrow 34_{0,34}$	$A_{1d} \leftarrow A_{1s}$ $A_{2d} \leftarrow A_{2s}$	204 081.212 204 076.883	204 079.047	−0.0395
$35_{1,34} \leftarrow 35_{0,35}$	$A_{1d} \leftarrow A_{1s}$ $A_{2d} \leftarrow A_{2s}$	204 179.992 204 175.651	204 177.822	−0.0175
$36_{1,35} \leftarrow 36_{0,36}$	$A_{1d} \leftarrow A_{1s}$ $A_{2d} \leftarrow A_{2s}$	204 281.507 204 277.136	204 279.321	−0.0221
$37_{1,36} \leftarrow 37_{0,37}$	$A_{1d} \leftarrow A_{1s}$ $A_{2d} \leftarrow A_{2s}$	204 385.750 204 381.378	204 383.564	−0.0273
$38_{1,37} \leftarrow 38_{0,38}$	$A_{1d} \leftarrow A_{1s}$ $A_{2d} \leftarrow A_{2s}$	204 492.743 204 488.371	204 490.557	−0.0210
$39_{1,38} \leftarrow 39_{0,39}$	$A_{1d} \leftarrow A_{1s}$ $A_{2d} \leftarrow A_{2s}$	204 602.487 204 598.071	204 600.279	−0.0177
$40_{1,39} \leftarrow 40_{0,40}$	$A_{1d} \leftarrow A_{1s}$ $A_{2d} \leftarrow A_{2s}$	204 714.941 204 710.514	204 712.727	−0.0139
$41_{1,40} \leftarrow 41_{0,41}$	$A_{1d} \leftarrow A_{1s}$ $A_{2d} \leftarrow A_{2s}$	204 830.105 204 825.669	204 827.887	−0.0169
$42_{1,41} \leftarrow 42_{0,42}$	$A_{1d} \leftarrow A_{1s}$ $A_{2d} \leftarrow A_{2s}$	204 948.013 204 943.545	204 945.779	0.0002
$43_{1,42} \leftarrow 43_{0,43}$	$A_{1d} \leftarrow A_{1s}$ $A_{2d} \leftarrow A_{2s}$	205 068.573 205 064.162	205 066.367	0.0086
$44_{1,43} \leftarrow 44_{0,44}$	$A_{1d} \leftarrow A_{1s}$ $A_{2d} \leftarrow A_{2s}$	205 191.927 205 187.398	205 189.663	0.0275
$46_{1,45} \leftarrow 46_{0,46}$	$A_{1d} \leftarrow A_{1s}$ $A_{2d} \leftarrow A_{2s}$	205 446.548 205 442.051	205 444.300	0.0477
$^pR_1$-branch transitions				
$19_{0,19} \leftarrow 18_{1,18}$	$A_{1d} \leftarrow A_{1s}$ $A_{2d} \leftarrow A_{2s}$	142 682.381 142 686.421	142 684.401	0.0314
$20_{0,20} \leftarrow 19_{1,19}$	$A_{1d} \leftarrow A_{1s}$ $A_{2d} \leftarrow A_{2s}$	160 864.911 160 869.323	160 867.117	−0.0200

(*continued*)

Table 5 (*continued*)

$J'_{K'_a,K'_c} \leftarrow J''_{K''_a,K''_c}$	$\Gamma'_{\text{tors}} \leftarrow \Gamma''_{\text{tors}}$	Measured transition/MHz	Centre frequency/MHz	$\nu_{\text{cent}} - \nu_{\text{calc.}}$/MHz
$^rQ_1$-branch transitions				
$5_{2,3} \leftarrow 5_{1,4}$	$A_{1s} \leftarrow A_{1d}$	606 432.652	606 434.222	0.0582
	$A_{2s} \leftarrow A_{2d}$	606 435.792		
$8_{2,6} \leftarrow 8_{1,7}$	$A_{1s} \leftarrow A_{1d}$	606 367.438	606 368.891	0.0159
	$A_{2s} \leftarrow A_{2d}$	606 370.344		
$10_{2,8} \leftarrow 10_{1,9}$	$A_{1s} \leftarrow A_{1d}$	606 308.279	606 309.911	0.1370
	$A_{2s} \leftarrow A_{2d}$	606 311.543		
$12_{2,10} \leftarrow 12_{1,11}$	$A_{1s} \leftarrow A_{1d}$	606 236.241	606 238.189	−0.0045
	$A_{2s} \leftarrow A_{2d}$	606 240.136		
$13_{2,11} \leftarrow 13_{1,12}$	$A_{1s} \leftarrow A_{1d}$	606 196.130	606 197.528	−0.1890
	$A_{2s} \leftarrow A_{2d}$	606 198.925		
$14_{2,12} \leftarrow 14_{1,13}$	$A_{1s} \leftarrow A_{1d}$	606 152.515	606 154.143	0.0315
	$A_{2s} \leftarrow A_{2d}$	606 155.770		
$16_{2,14} \leftarrow 16_{1,15}$	$A_{1s} \leftarrow A_{1d}$	606 055.701	606 057.341	−0.1630
	$A_{2s} \leftarrow A_{2d}$	606 058.981		
$17_{2,15} \leftarrow 17_{1,16}$	$A_{1s} \leftarrow A_{1d}$	606 002.820	606 004.655	0.1600
	$A_{2s} \leftarrow A_{2d}$	606 006.490		
$18_{2,16} \leftarrow 18_{1,17}$	$A_{1s} \leftarrow A_{1d}$	605 946.695	605 948.354	0.0100
	$A_{2s} \leftarrow A_{2d}$	605 950.013		
$19_{2,17} \leftarrow 19_{1,18}$	$A_{1s} \leftarrow A_{1d}$	605 887.453	605 888.958	−0.0894
	$A_{2s} \leftarrow A_{2d}$	605 890.463		
$21_{2,19} \leftarrow 2_{1,20}$	$A_{1s} \leftarrow A_{1d}$	605 759.490	605 760.946	0.0552
	$A_{2s} \leftarrow A_{2d}$	605 762.403		
$23_{2,21} \leftarrow 23_{1,22}$	$A_{1s} \leftarrow A_{1d}$	605 618.695	605 620.388	0.0653
	$A_{2s} \leftarrow A_{2d}$	605 622.081		
$24_{2,22} \leftarrow 24_{1,23}$	$A_{1s} \leftarrow A_{1d}$	605 543.626	605 545.166	−0.0694
	$A_{2s} \leftarrow A_{2d}$	605 546.706		
$25_{2,23} \leftarrow 25_{1,24}$	$A_{1s} \leftarrow A_{1d}$	605 465.378	605 466.925	−0.0515
	$A_{2s} \leftarrow A_{2d}$	605 468.471		
$27_{2,25} \leftarrow 27_{1,26}$	$A_{1s} \leftarrow A_{1d}$	605 299.304	605 300.870	−0.0554
	$A_{2s} \leftarrow A_{2d}$	605 302.436		
$28_{2,26} \leftarrow 28_{1,27}$	$A_{1s} \leftarrow A_{1d}$	605 211.446	605 213.114	−0.0095
	$A_{2s} \leftarrow A_{2d}$	605 214.782		
$30_{2,28} \leftarrow 30_{1,29}$	$A_{1s} \leftarrow A_{1d}$	605 026.271	605 027.951	0.0080
	$A_{2s} \leftarrow A_{2d}$	605 029.630		
$32_{2,30} \leftarrow 32_{1,31}$	$A_{1s} \leftarrow A_{1d}$	604 828.383	604 829.984	0.0234
	$A_{2s} \leftarrow A_{2d}$	604 831.586		
$33_{2,31} \leftarrow 33_{1,32}$	$A_{1s} \leftarrow A_{1d}$	604 724.559	604 726.170	0.0136
	$A_{2s} \leftarrow A_{2d}$	604 727.780		
$35_{2,33} \leftarrow 35_{1,34}$	$A_{1s} \leftarrow A_{1d}$	604 507.264	604 508.910	0.0124
	$A_{2s} \leftarrow A_{2d}$	604 510.556		
$36_{2,34} \leftarrow 36_{1,35}$	$A_{1s} \leftarrow A_{1d}$	604 393.892	604 395.487	0.0535
	$A_{2s} \leftarrow A_{2d}$	604 397.082		

Table 5 (*continued*)

$J'_{K'_a,K'_c} \leftarrow J''_{K''_a,K''_c}$	$\Gamma'_{\text{tors}} \leftarrow \Gamma''_{\text{tors}}$	Measured transition/MHz	Centre frequency/MHz	$\nu_{\text{cent}} - \nu_{\text{calc.}}$/MHz
$38_{2,36} \leftarrow 38_{1,37}$	$A_{1s} \leftarrow A_{1d}$ $A_{2s} \leftarrow A_{2d}$	604 157.075 604 160.348	604 158.711	−0.1010
$39_{2,37} \leftarrow 39_{1,38}$	$A_{1s} \leftarrow A_{1d}$ $A_{2s} \leftarrow A_{2d}$	604 034.252 604 037.610	604 035.931	0.2840
$40_{2,38} \leftarrow 40_{1,39}$	$A_{1s} \leftarrow A_{1d}$ $A_{2s} \leftarrow A_{2d}$	603 907.420 603 910.695	603 909.058	−0.1800
$41_{2,39} \leftarrow 41_{1,40}$	$A_{1s} \leftarrow A_{1d}$ $A_{2s} \leftarrow A_{2d}$	603 777.974 603 781.068	603 779.521	−0.0613
$43_{2,41} \leftarrow 43_{1,42}$	$A_{1s} \leftarrow A_{1d}$ $A_{2s} \leftarrow A_{2d}$	603 508.900 603 512.190	603 510.545	0.0300
$8_{2,7} \leftarrow 8_{1,8}$	$A_{1s} \leftarrow A_{1d}$ $A_{2s} \leftarrow A_{2d}$	606 577.525 606 580.192	606 578.858	−0.0990
$9_{2,8} \leftarrow 9_{1,9}$	$A_{1s} \leftarrow A_{1d}$ $A_{2s} \leftarrow A_{2d}$	606 602.127 606 604.972	606 603.550	0.0220
$10_{2,9} \leftarrow 10_{1,10}$	$A_{1s} \leftarrow A_{1d}$ $A_{2s} \leftarrow A_{2d}$	606 629.451 606 632.357	606 630.904	0.0628
$11_{2,10} \leftarrow 11_{1,11}$	$A_{1s} \leftarrow A_{1d}$ $A_{2s} \leftarrow A_{2d}$	606 659.643 606 662.423	606 661.033	0.1330
$12_{2,11} \leftarrow 12_{1,12}$	$A_{1s} \leftarrow A_{1d}$ $A_{2s} \leftarrow A_{2d}$	606 692.257 606 695.048	606 693.653	−0.0566
$13_{2,12} \leftarrow 13_{1,13}$	$A_{1s} \leftarrow A_{1d}$ $A_{2s} \leftarrow A_{2d}$	606 727.826 606 730.742	606 729.284	0.0104
$14_{2,13} \leftarrow 14_{1,14}$	$A_{1s} \leftarrow A_{1d}$ $A_{2d} \leftarrow A_{2s}$	606 766.074 606 768.995	606 767.535	−0.0619
$15_{2,14} \leftarrow 15_{1,15}$	$A_{1s} \leftarrow A_{1d}$ $A_{2s} \leftarrow A_{2d}$	606 807.204 606 810.084	606 808.644	−0.0409
$16_{2,15} \leftarrow 16_{1,16}$	$A_{1s} \leftarrow A_{1d}$ $A_{2s} \leftarrow A_{2d}$	606 850.978 606 853.994	606 852.486	−0.0570
$18_{2,17} \leftarrow 18_{1,18}$	$A_{1s} \leftarrow A_{1d}$ $A_{2s} \leftarrow A_{2d}$	606 947.035 606 949.883	606 948.459	−0.1340
$20_{2,19} \leftarrow 20_{1,20}$	$A_{1s} \leftarrow A_{1d}$ $A_{2s} \leftarrow A_{2d}$	607 054.728 607 057.189	607 055.958	0.1610
$21_{2,20} \leftarrow 21_{1,21}$	$A_{1s} \leftarrow A_{1d}$ $A_{2s} \leftarrow A_{2d}$	607 112.227 607 114.942	607 113.585	−0.0140
$22_{2,21} \leftarrow 22_{1,22}$	$A_{1s} \leftarrow A_{1d}$ $A_{2s} \leftarrow A_{2d}$	607 172.655 607 175.652	607 174.154	−0.0563
$23_{2,22} \leftarrow 23_{1,23}$	$A_{1s} \leftarrow A_{1d}$ $A_{2s} \leftarrow A_{2d}$	607 236.106 607 239.685	607 237.895	0.2570
$24_{2,23} \leftarrow 24_{1,24}$	$A_{1s} \leftarrow A_{1d}$ $A_{2s} \leftarrow A_{2d}$	607 302.395 607 305.201	607 303.798	−0.0933
$25_{2,24} \leftarrow 25_{1,25}$	$A_{1s} \leftarrow A_{1d}$ $A_{2s} \leftarrow A_{2d}$	607 371.521 607 374.212	607 372.867	−0.1100

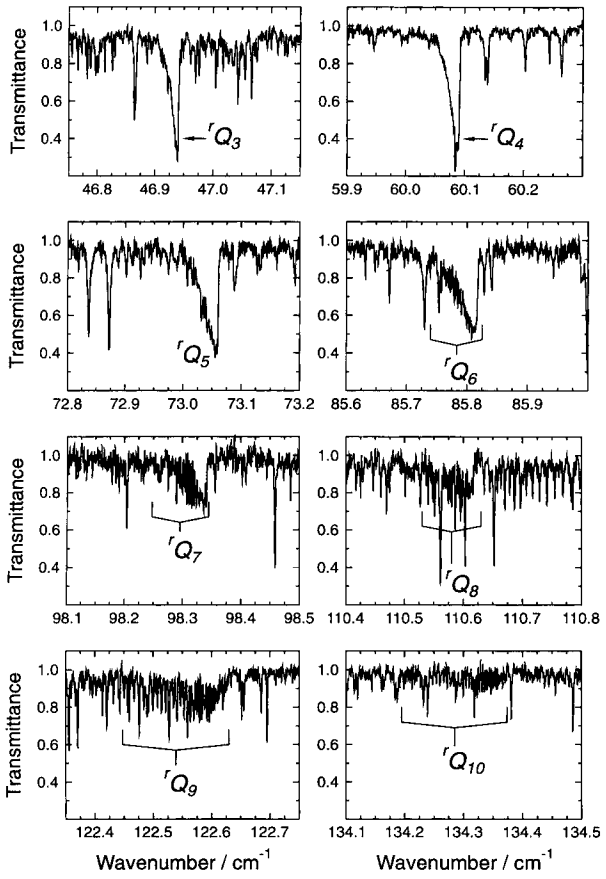

Figure 8. $^rQ_{K_a}$ branches of DNCND in the far infrared region. Due to their characteristic appearance they play a key role in the identification of DNCND transitions among the dense transitions of the D_2NCN spectrum.

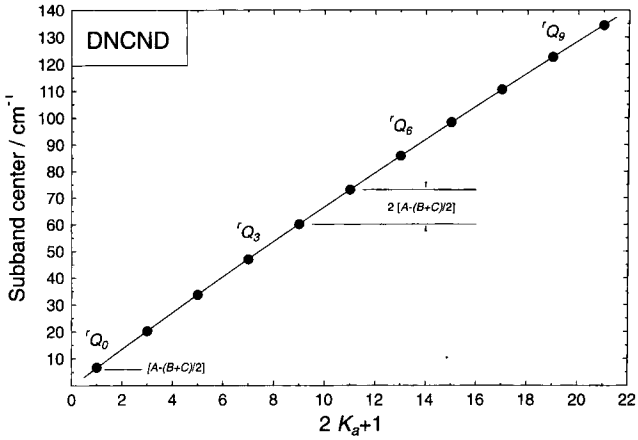

Figure 9. Plot of the subband centres of DNCND subbranches versus $(2K_a + 1)$, which shows the regular linear behaviour of an unperturbed perpendicular band system.

An example for these transitions is presented in figure 10, and the assigned line positions are given in table 6. Overlaps with strong D_2NCN transitions are again frequent. Some $^rR_2$-branch lines were also observed. However, they are omitted in table 6 due to their low intensities and large errors caused by the overlap with cyanamide transitions.

Neither asymmetry splitting nor torsional splittings are observed for DNCND lines assigned in the FIR region. The asymmetry splitting collapses, of course, with increasing K_a. The torsional splitting also collapses, because the rotation about the *a* axis produces a centrifugal force which effectively increases the torsional barrier [3].

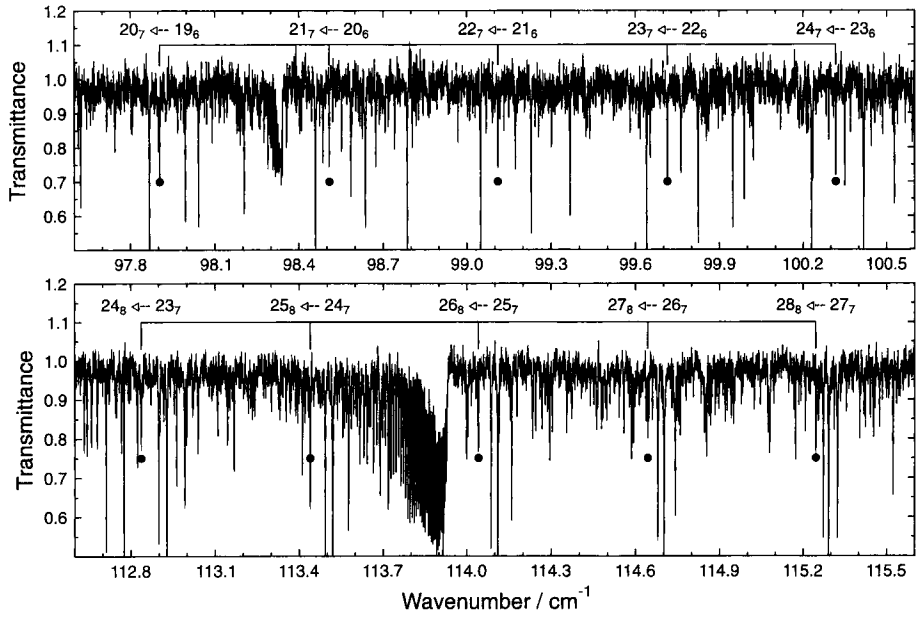

Figure 10. Part of two $^rR_{K_a}$ branches of DNCND in the far infrared region. Nearly all of the strong lines belong to the D_2NCN molecule.

Table 6. Assigned transitions of DNCND in the FIR region. The measured wavenumbers, which show no asymmetry or torsional splitting, were fitted together with the data of table 5 to the Watson Hamiltonian in *S* reduction. The wavenumber differences between the observed transitions and those calculated with the constants of table 7 are also listed.

$J_{K_a'} \leftarrow J_{K_a''}$	Measured transtions /cm^{-1}	$\tilde{\nu}_{obs.} - \tilde{\nu}_{calc}$ $\times 10^3$/cm^{-1}	$J_{K_a'} \leftarrow J_{K_a''}$	Measured transions /cm^{-1}	$\tilde{\nu}_{obs.} - \tilde{\nu}_{calc}$ $\times 10^3$/cm^{-1}	$J_{K_a'} \leftarrow J_{K_a''}$	Measured transitions /cm^{-1}	$\tilde{\nu}_{obs.} - \tilde{\nu}_{calc}$ $\times 10^3$/cm^{-1}
$^rR_3$-branch transitions, $A_s \leftarrow A_d$								
$4_4 \leftarrow 3_3$	49.360 888	−0.416	$5_4 \leftarrow 4_3$	49.965 848	−0.376	$6_4 \leftarrow 5_3$	50.570 951	−0.163
$7_4 \leftarrow 6_3$	51.176 040	0.067	$8_4 \leftarrow 7_3$	51.780 777	−0.021	$9_4 \leftarrow 8_3$	52.385 525	−0.063
$10_4 \leftarrow 9_3$	52.990 037	−0.302	$11_4 \leftarrow 10_3$	53.595 092	0.041	$12_4 \leftarrow 11_3$	54.199 671	−0.049
$13_4 \leftarrow 12_3$	54.804 387	0.042	$14_4 \leftarrow 13_3$	55.408 722	−0.201	$15_4 \leftarrow 14_3$	56.013 427	−0.025
$16_4 \leftarrow 15_3$	56.618 022	0.091	$17_4 \leftarrow 16_3$	57.222 289	−0.067	$18_4 \leftarrow 17_3$	57.826 786	0.060
$19_4 \leftarrow 18_3$	58.431 067	0.028	$20_4 \leftarrow 19_3$	59.035 321	0.029	$22_4 \leftarrow 21_3$	60.243 528	−0.082
$23_4 \leftarrow 22_3$	60.847 610	−0.060	$24_4 \leftarrow 23_3$	61.451 541	−0.121	$25_4 \leftarrow 24_3$	62.055 438	−0.146
$26_4 \leftarrow 25_3$	62.659 493	0.060	$27_4 \leftarrow 26_3$	63.263 013	−0.194	$28_4 \leftarrow 27_3$	63.866 894	−0.010
$29_4 \leftarrow 28_3$	64.470 537	0.016	$30_3 \leftarrow 29_3$	65.074 168	0.111	$31_4 \leftarrow 30_3$	65.677 471	−0.038
$32_4 \leftarrow 31_3$	66.280 628	−0.247	$33_4 \leftarrow 32_3$	66.884 160	0.006	$34_4 \leftarrow 33_3$	67.487 083	−0.259
$35_4 \leftarrow 34_3$	68.090 298	−0.139	$36_4 \leftarrow 35_3$	68.693 100	−0.338	$39_4 \leftarrow 38_3$	70.501 874	0.023
$40_4 \leftarrow 39_3$	71.104 084	−0.367	$41_4 \leftarrow 40_3$	71.706 652	−0.294	$43_4 \leftarrow 42_3$	72.911 650	0.040
$^rR_4$-branch transitions, $A_d \leftarrow A_s$								
$5_4 \leftarrow 4_4$	63.117 351	0.015	$6_5 \leftarrow 5_4$	63.722 215	0.060	$7_5 \leftarrow 6_4$	64.326 997	0.063
$8_5 \leftarrow 7_4$	64.931 693	0.022	$9_5 \leftarrow 8_4$	65.536 482	0.119	$10_5 \leftarrow 9_4$	66.141 094	0.086
$11_5 \leftarrow 10_4$	66.745 700	0.095	$12_5 \leftarrow 11_4$	67.350 285	0.134	$13_5 \leftarrow 12_4$	67.954 794	0.151
$14_5 \leftarrow 13_4$	68.559 154	0.074	$15_5 \leftarrow 14_4$	69.163 574	0.115	$16_5 \leftarrow 15_4$	69.767 873	0.094
$17_5 \leftarrow 16_4$	70.372 201	0.164	$18_5 \leftarrow 17_4$	70.976 269	0.039	$19_5 \leftarrow 18_4$	71.580 644	0.287
$20_5 \leftarrow 19_4$	72.184 698	0.282	$21_5 \leftarrow 20_4$	72.788 530	0.125	$22_5 \leftarrow 21_4$	73.392 501	0.181
$23_5 \leftarrow 22_4$	73.996 227	0.067	$24_5 \leftarrow 23_4$	74.599 726	−0.198	$25_5 \leftarrow 24_4$	75.203 509	−0.099
$26_5 \leftarrow 25_4$	75.807 134	−0.076	$27_5 \leftarrow 26_4$	76.410 765	0.036	$28_5 \leftarrow 27_4$	77.013 952	−0.210
$29_5 \leftarrow 28_4$	77.617 411	−0.096	$31_5 \leftarrow 30_4$	78.824 046	0.122	$32_5 \leftarrow 31_4$	79.427 123	0.132
$33_5 \leftarrow 32_4$	80.030 026	0.064	$34_5 \leftarrow 33_4$	80.632 963	0.129	$35_5 \leftarrow 34_4$	81.235 584	−0.021
$36_5 \leftarrow 35_4$	81.838 457	0.184	$37_5 \leftarrow 36_4$	82.441 048	0.213	$38_5 \leftarrow 37_4$	83.043 525	0.236
$39_5 \leftarrow 38_4$	83.645 097	−0.537	$40_5 \leftarrow 39_4$	84.247 733	−0.134	$41_5 \leftarrow 40_4$	84.849 798	−0.187
$42_5 \leftarrow 41_4$	85.451 490	−0.497	$43_5 \leftarrow 42_4$	86.054 216	0.345	$44_5 \leftarrow 43_4$	86.655 547	−0.087
$^rR_5$-branch transitions, $A_s \leftarrow A_d$								
$6_6 \leftarrow 5_5$	76.690 714	0.161	$7_6 \leftarrow 6_5$	77.295 523	0.298	$8_6 \leftarrow 7_5$	77.900 007	0.164
$9_6 \leftarrow 8_5$	78.504 722	0.318	$10_6 \leftarrow 9_5$	79.109 100	0.192	$11_6 \leftarrow 10_5$	79.713 379	0.027
$12_6 \leftarrow 11_5$	80.317 774	0.041	$13_6 \leftarrow 12_5$	80.922 218	0.169	$14_6 \leftarrow 13_5$	81.526 404	0.105
$15_6 \leftarrow 14_5$	82.130 513	0.034	$16_6 \leftarrow 15_5$	82.734 808	0.220	$17_6 \leftarrow 16_5$	83.338 759	0.135
$18_6 \leftarrow 17_5$	83.942 717	0.132	$19_6 \leftarrow 18_5$	84.546 760	0.293	$20_6 \leftarrow 19_5$	85.150 369	0.099
$21_6 \leftarrow 20_5$	85.754 226	0.235	$22_6 \leftarrow 21_5$	86.357 808	0.181	$23_6 \leftarrow 22_5$	86.961 429	0.252
$25_6 \leftarrow 24_5$	88.168 126	0.117	$26_6 \leftarrow 25_5$	88.771 731	0.444	$27_6 \leftarrow 26_5$	89.374 722	0.252
$28_6 \leftarrow 27_5$	89.977 574	0.019	$29_6 \leftarrow 28_5$	90.580 669	0.128	$30_6 \leftarrow 29_5$	91.183 573	0.148
$31_6 \leftarrow 30_5$	91.786 608	0.403	$32_6 \leftarrow 31_5$	92.388 824	−0.055	$33_6 \leftarrow 32_5$	92.991 512	0.067
$34_6 \leftarrow 33_5$	93.593 251	−0.650	$35_6 \leftarrow 34_5$	94.196 547	0.303	$36_6 \leftarrow 35_5$	94.798 271	−0.202
$37_6 \leftarrow 36_5$	95.400 346	−0.238	$38_6 \leftarrow 37_5$	96.002 493	−0.084	$39_6 \leftarrow 38_5$	96.604 431	−0.017
$40_6 \leftarrow 39_5$	97.205 928	−0.268	$41_6 \leftarrow 40_5$	97.807 528	−0.290	$42_6 \leftarrow 41_5$	98.409 320	0.007
$43_6 \leftarrow 42_5$	99.010 458	−0.219	$44_6 \leftarrow 43_5$	99.611 828	−0.082	$45_6 \leftarrow 44_5$	100.212 332	−0.676
$46_6 \leftarrow 45_5$	100.814 096	0.127	$47_6 \leftarrow 46_5$	101.414 887	0.095	$48_6 \leftarrow 47_5$	102.015 110	−0.364
$^rR_6$-branch transitions, $A_d \leftarrow A_s$								
$7_7 \leftarrow 6_6$	90.052 909	−0.006	$9_7 \leftarrow 8_6$	91.261 734	−0.034	$10_7 \leftarrow 9_6$	91.865 992	−0.094
$11_7 \leftarrow 10_6$	92.470 399	0.070	$12_7 \leftarrow 11_6$	93.074 414	−0.081	$13_7 \leftarrow 12_6$	93.678 355	−0.226
$14_7 \leftarrow 13_6$	94.282 654	0.068	$15_7 \leftarrow 14_6$	94.886 309	−0.199	$16_7 \leftarrow 15_6$	95.490 149	−0.194
$18_7 \leftarrow 17_6$	96.697 742	−0.005	$19_7 \leftarrow 18_6$	97.301 202	−0.110	$20_7 \leftarrow 19_6$	97.904 691	−0.091
$21_7 \leftarrow 20_6$	98.508 114	−0.041	$22_7 \leftarrow 21_6$	99.111 159	−0.271	$23_7 \leftarrow 22_6$	99.714 346	−0.257
$24_7 \leftarrow 23_6$	100.317 703	0.030	$25_7 \leftarrow 24_6$	100.920 504	−0.133	$26_7 \leftarrow 25_6$	101.523 381	−0.113
$28_7 \leftarrow 27_6$	102.728 877	0.002	$29_7 \leftarrow 28_6$	103.331 551	0.155	$30_7 \leftarrow 29_6$	103.933 858	0.057

(*continued*)

Table 6 (*continued*)

$J_{K_a'} \leftarrow J_{K_a''}$	Measured transitions /cm^{-1}	$\tilde{\nu}_{obs.} - \tilde{\nu}_{calc}$ $\times 10^3$/cm^{-1}	$J_{K_a'} \leftarrow J_{K_a''}$	Measured transitions /cm^{-1}	$\tilde{\nu}_{obs.} - \tilde{\nu}_{calc}$ $\times 10^3$/cm^{-1}	$J_{K_a'} \leftarrow J_{K_a''}$	Measured transitions /cm^{-1}	$\tilde{\nu}_{obs.} - \tilde{\nu}_{calc}$ $\times 10^3$/cm^{-1}
$31_7 \leftarrow 30_6$	104.536 091	0.005	$33_7 \leftarrow 32_6$	105.740 033	−0.261	$34_7 \leftarrow 33_6$	106.342 121	−0.090
$35_7 \leftarrow 34_6$	106.943 889	−0.112	$36_7 \leftarrow 35_6$	107.545 818	0.157	$37_7 \leftarrow 36_6$	108.146 935	−0.255
$38_7 \leftarrow 37_6$	108.748 704	0.119	$39_7 \leftarrow 38_6$	109.349 906	0.061	$40_7 \leftarrow 39_6$	109.950 725	−0.241
$41_7 \leftarrow 40_6$	110.551 514	−0.432	$43_7 \leftarrow 42_6$	111.753 625	0.147	$44_7 \leftarrow 43_6$	112.354 172	0.147
$45_7 \leftarrow 44_6$	112.954 357	−0.066	$46_7 \leftarrow 45_6$	113.554 806	0.136	$47_7 \leftarrow 46_6$	114.155 040	0.277
$^rR_7$-branch transitions, $A_s \leftarrow A_d$								
$8_8 \leftarrow 7_7$	103.181 903	−0.090	$9_8 \leftarrow 8_7$	103.785 908	−0.256	$10_8 \leftarrow 9_7$	104.390 197	−0.046
$11_8 \leftarrow 10_7$	104.994 452	0.223	$12_8 \leftarrow 11_7$	105.597 847	−0.272	$13_8 \leftarrow 12_7$	106.201 699	−0.212
$14_8 \leftarrow 13_7$	106.805 445	−0.158	$15_8 \leftarrow 14_7$	107.409 143	−0.050	$16_5 \leftarrow 15_7$	108.012 665	−0.013
$17_8 \leftarrow 16_7$	108.615 927	−0.129	$18_8 \leftarrow 17_7$	109.219 045	−0.281	$18_8 \leftarrow 18_7$	109.822 160	−0.325
$20_8 \leftarrow 19_7$	110.425 481	−0.049	$21_8 \leftarrow 20_7$	111.028 469	0.008	$22_8 \leftarrow 21_7$	111.631 183	−0.090
$24_8 \leftarrow 23_7$	112.836 776	0.238	$25_8 \leftarrow 24_7$	113.438 985	0.000	$26_8 \leftarrow 25_7$	114.041 353	0.047
$27_8 \leftarrow 26_7$	114.643 399	−0.099	$28_8 \leftarrow 27_7$	115.245 382	−0.178	$30_8 \leftarrow 29_7$	116.449 168	−0.116
$33_8 \leftarrow 32_7$	118.253 975	0.139	$34_8 \leftarrow 33_7$	118.855 458	0.389	$35_8 \leftarrow 34_7$	119.456 147	−0.009
$36_8 \leftarrow 35_7$	120.057 306	0.211	$37_8 \leftarrow 36_7$	120.657 956	0.072	$38_8 \leftarrow 37_7$	121.258 538	0.017
$39_8 \leftarrow 38_7$	121.859 340	0.337	$40_8 \leftarrow 39_7$	122.459 502	0.174	$41_8 \leftarrow 40_7$	123.059 797	0.302
$42_8 \leftarrow 41_7$	123.659 866	0.365	$43_8 \leftarrow 42_7$	124.259 675	0.332	$44_8 \leftarrow 43_7$	124.859 492	0.472
$45_8 \leftarrow 44_7$	125.458 890	0.360						
$^rR_8$-branch transitions, $A_d \leftarrow A_s$								
$10_9 \leftarrow 9_8$	116.664 469	0.007	$11_9 \leftarrow 10_8$	117.267 803	−0.320	$12_9 \leftarrow 11_8$	117.871 419	−0.246
$13_9 \leftarrow 12_8$	118.474 787	−0.299	$14_9 \leftarrow 13_8$	119.078 214	−0.170	$15_9 \leftarrow 14_8$	119.681 240	−0.317
$16_9 \leftarrow 15_8$	120.284 423	−0.179	$17_9 \leftarrow 16_8$	120.887 349	−0.169	$20_9 \leftarrow 19_8$	122.695 413	−0.052
$21_9 \leftarrow 20_8$	123.297 642	−0.199	$22_9 \leftarrow 21_8$	123.899 924	−0.152	$23_9 \leftarrow 22_8$	124.501 777	−0.391
$24_9 \leftarrow 23_8$	125.104 079	−0.036	$25_9 \leftarrow 24_8$	125.705 829	−0.087	$26_9 \leftarrow 25_8$	126.307 550	−0.017
$27_9 \leftarrow 26_8$	126.909 149	0.082	$28_9 \leftarrow 27_8$	127.510 476	0.063	$29_9 \leftarrow 28_8$	128.111 523	−0.080
$30_9 \leftarrow 29_8$	128.712 401	−0.235	$31_9 \leftarrow 30_8$	129.313 595	0.087	$32_9 \leftarrow 31_8$	129.914 445	0.227
$34_9 \leftarrow 33_8$	131.115 078	−0.065	$35_9 \leftarrow 34_8$	131.714 653	−0.700	$36_9 \leftarrow 35_8$	132.315 545	0.152
$37_9 \leftarrow 36_8$	132.915 432	0.173	$38_9 \leftarrow 37_8$	133.515 311	0.361	$39_9 \leftarrow 38_8$	134.114 517	0.054
$40_9 \leftarrow 39_8$	134.714 032	0.235	$42_9 \leftarrow 41_8$	135.912 454	0.537	$43_9 \leftarrow 42_8$	136.511 177	0.478
$^rR_9$-branch transitions, $A_s \leftarrow A_d$								
$10_{10} \leftarrow 9_9$	128.676 823	0.019	$11_{10} \leftarrow 10_9$	129.279 997	−0.065	$12_{10} \leftarrow 11_9$	129.883 165	−0.008
$13_{10} \leftarrow 12_9$	130.486 050	−0.085	$15_{10} \leftarrow 14_9$	131.691 651	0.048	$16_{10} \leftarrow 15_9$	132.294 058	−0.047
$17_{10} \leftarrow 16_9$	132.896 491	0.042	$18_{10} \leftarrow 17_9$	133.498 565	−0.069	$19_{10} \leftarrow 18_9$	134.100 566	−0.090
$20_{10} \leftarrow 19_9$	134.702 387	−0.127	$21_{10} \leftarrow 20_9$	135.304 216	0.010	$22_{10} \leftarrow 21_9$	135.905 464	−0.265
$23_{10} \leftarrow 22_9$	136.507 059	−0.023	$24_{10} \leftarrow 23_9$	137.108 185	−0.077	$25_{10} \leftarrow 24_9$	137.709 033	−0.233
$26_{10} \leftarrow 25_9$	138.310 216	0.122	$27_{10} \leftarrow 26_9$	138.910 741	−0.000	$28_{10} \leftarrow 27_9$	139.511 241	0.033
$29_{10} \leftarrow 28_9$	140.111 701	0.210	$31_{10} \leftarrow 30_9$	141.311 567	0.071	$32_{10} \leftarrow 31_9$	141.911 527	0.313
$33_{10} \leftarrow 32_9$	142.510 736	−0.004	$34_{10} \leftarrow 33_9$	143.110 251	0.180	$35_{10} \leftarrow 34_9$	143.709 387	0.181
$36_{10} \leftarrow 35_9$	144.308 199	0.058	$37_{10} \leftarrow 36_9$	144.907 240	0.365	$38_{10} \leftarrow 37_9$	145.505 617	0.211
$^rQ_9$-branch transitions, $A_s \leftarrow A_d$								
$13_{10} \leftarrow 13_9$	122.625 920	0.468	$14_{10} \leftarrow 14_9$	122.624 073	0.341	$15_{10} \leftarrow 15_9$	122.621 966	0.077
$16_{10} \leftarrow 16_9$	122.619 928	0.005	$17_{10} \leftarrow 17_9$	122.617 538	−0.296	$18_{10} \leftarrow 18_9$	122.615 399	−0.223
$19_{10} \leftarrow 19_9$	122.613 122	−0.166	$20_{10} \leftarrow 20_9$	122.610 838	0.007	$21_{10} \leftarrow 21_9$	122.607 984	−0.266
$22_{10} \leftarrow 22_9$	122.605 620	0.073	$23_{10} \leftarrow 23_9$	122.603 003	0.282	$24_{10} \leftarrow 24_9$	122.600 083	0.310
$25_{10} \leftarrow 25_9$	122.596 476	−0.225	$26_{10} \leftarrow 26_9$	122.592 735	−0.771			
$^rR_{10}$-branch transitions, $A_d \leftarrow A_s$								
$11_{11} \leftarrow 10_{10}$	141.023 180	0.223	$12_{11} \leftarrow 11_{10}$	141.625 828	0.287	$13_{11} \leftarrow 12_{10}$	142.228 330	0.387
$14_{11} \leftarrow 13_{10}$	142.830 491	0.332	$15_{11} \leftarrow 14_{10}$	143.432 258	0.069	$16_{11} \leftarrow 15_{10}$	144.034 337	0.308
$17_{11} \leftarrow 16_{10}$	144.635 834	0.155	$18_{11} \leftarrow 17_{10}$	145.237 066	−0.068	$19_{11} \leftarrow 18_{10}$	145.838 383	−0.011
$20_{11} \leftarrow 19_{10}$	146.439 649	0.192	$21_{11} \leftarrow 20_{10}$	147.040 887	0.568	$23_{11} \leftarrow 22_{10}$	148.241 815	0.381

Table 6 (*continued*)

$J_{K_a'} \leftarrow J_{K_a''}$	Measured transitions /cm^{-1}	$\tilde{\nu}_{obs.} - \tilde{\nu}_{calc}$ $\times 10^3$/cm^{-1}	$J_{K_a'} \leftarrow J_{K_a''}$	Measured transitions /cm^{-1}	$\tilde{\nu}_{obs.} - \tilde{\nu}_{calc}$ $\times 10^3$/cm^{-1}	$J_{K_a'} \leftarrow J_{K_a''}$	Measured transitions /cm^{-1}	$\tilde{\nu}_{obs.} - \tilde{\nu}_{calc}$ $\times 10^3$/cm^{-1}
$25_{11} \leftarrow 24_{10}$	149.441 642	−0.082	$26_{11} \leftarrow 25_{10}$	150.041 538	−0.015	$27_{11} \leftarrow 26_{10}$	150.640 741	−0.428
$28_{11} \leftarrow 27_{10}$	151.240 395	−0.175	$29_{11} \leftarrow 28_{10}$	151.839 846	0.092	$30_{11} \leftarrow 29_{10}$	152.438 507	−0.211
$31_{11} \leftarrow 30_{10}$	153.037 243	−0.217	$32_{11} \leftarrow 31_{10}$	153.635 715	−0.264	$33_{11} \leftarrow 32_{10}$	154.233 970	−0.301
$34_{11} \leftarrow 33_{10}$	154.832 087	−0.248	$35_{11} \leftarrow 34_{10}$	155.429 894	−0.274	$36_{11} \leftarrow 35_{10}$	156.027 551	−0.218
$37_{11} \leftarrow 36_{10}$	156.624 799	−0.336	$38_{11} \leftarrow 37_{10}$	157.222 606	0.342	$39_{11} \leftarrow 38_{10}$	157.819 036	−0.117
$40_{11} \leftarrow 39_{10}$	158.415 512	−0.290	$41_{11} \leftarrow 40_{10}$	159.012 085	−0.122	$42_{11} \leftarrow 41_{10}$	159.608 432	0.066
$43_{11} \leftarrow 42_{10}$	160.204 642	0.365	$44_{11} \leftarrow 43_{10}$	160.799 369	−0.569			
$^rQ_{10}$-branch transitions, $A_d \leftarrow A_s$								
$11_{11} \leftarrow 11_{10}$	134.373 351	0.581	$12_{11} \leftarrow 12_{10}$	134.371 351	0.459	$13_{11} \leftarrow 13_{10}$	134.369 368	0.511
$14_{11} \leftarrow 14_{10}$	134.367 094	0.428	$15_{11} \leftarrow 15_{10}$	134.364 408	0.090	$16_{11} \leftarrow 16_{10}$	134.361 952	0.139
$17_{11} \leftarrow 17_{10}$	134.359 071	−0.081	$18_{11} \leftarrow 18_{10}$	134.356 446	0.111	$19_{11} \leftarrow 19_{10}$	134.352 993	−0.368
$20_{11} \leftarrow 20_{10}$	134.350 542	0.312	$21_{11} \leftarrow 21_{10}$	134.347 241	0.298	$22_{11} \leftarrow 22_{10}$	134.343 548	0.048
$23_{11} \leftarrow 23_{10}$	134.339 815	−0.085	$24_{11} \leftarrow 24_{10}$	134.336 014	−0.129	$25_{11} \leftarrow 25_{10}$	134.332 108	−0.122
$26_{11} \leftarrow 26_{10}$	134.328 088	−0.072	$27_{11} \leftarrow 27_{10}$	134.323 867	−0.067	$28_{11} \leftarrow 28_{10}$	134.318 966	−0.585
$29_{11} \leftarrow 29_{10}$	134.314 675	−0.337	$30_{11} \leftarrow 30_{10}$	134.310 129	−0.187	$31_{11} \leftarrow 31_{10}$	134.304 709	−0.755

In order to determine the rotational constants for the isotopomers of HNCNH, a separation of the torsional from the rotational information is needed. The unperturbed position of the pure rotational transition is given by the centre of each torsional–rotational doublet, since both components have the same statistical weight. The resulting line positions were then fitted to the constants of the Watson Hamiltonian in S reduction (I^r representation) [21, 22]. The matrix elements in the basis of the prolate symmetric top wavefunctions $|JK_a\rangle$, including the constants relevant to this work, are as follows:

$$\begin{aligned}\frac{E_{K_a,K_a}}{h} &= \tfrac{1}{2}(B+C)J(J+1) + \left[A - \tfrac{1}{2}(B+C)\right]K_a^2 \\ &\quad - D_J J^2(J+1)^2 - D_{JK}J(J+1)K_a^2 \\ &\quad - D_K K_a^4 + H_{KJ}J(J+1)K_a^4 + H_K K_a^6 \\ &\quad - L_{KJ}J(J+1)K_a^6 - L_K K_a^8 + S_{KJ}J(J+1)K_a^8 \\ &\quad + S_K K_a^{10} - T_{KJ}J(J+1)K_a^{10} \\ &\quad - T_K K_a^{12} + U_K K_a^{14}\,, \qquad (3)\end{aligned}$$

$$\begin{aligned}\frac{W_{K_a,K_a\pm2}}{h} &= \tfrac{1}{4}[(B-C) + d_1 J(J+1)] \\ &\quad \times \{f(J,K_a,0)f(J,K_a,1)\}, \qquad (4)\end{aligned}$$

$$\frac{V_{K_a,K_a\pm4}}{h} = \{d_2 + h_2 J(J+1)\}\prod_{l=0}^{3} f(J,K_a,l), \qquad (5)$$

with

$$f(J,K_a,l) = [J(J+1) - (K_a \pm l)(K_a \pm l)(K_a \pm l \pm 1)]^{1/2}\,. \qquad (6)$$

A, B, C are the rotational constants, while all the other constants are centrifugal distortion constants.

The adjusted constants are given in table 7 for four isotopomers of HNCNH. The data for the fit of the main species were taken from [1, 4, 5]. ([5] reports only spectroscopic constants for each torsional symmetry species separately.) Due to the limited data available for the $H^{15}NC^{15}NH$ and $HN^{13}CNH$, species, the constants D_K, H_K, H_{KJ} and d_2 were held fixed in the fits at the values found for the main species. Ray's asymmetry parameter κ is also listed in table 8 (see section 5) for the four isotopomers.

4. Discussion of the rotational analysis, torsional splitting and K_a doubling

The most outstanding feature observed upon comparing the spectroscopic constants of the four HNCNH isotopomers, going from the main species to DNCND, is the decreasing trend of the A rotational constants and of the D_{JK} and D_K centrifugal distortion constants which describe the K_a-dependent parts in the Hamiltonian. Lines with higher K_a values are included in the DNCND fit compared with HNCNH (DNCND: $K_a^{max} = 11$, HNCNH: $K_a^{max} = 10$). However, higher order constants are necessary in the fit of the main species.

It is interesting to follow the changes in the torsional splittings and their J dependence for the various isotopomers of HNCNH, as plotted in figure 11. With higher mass, compared with the main species, the splitting decreases. For the deuterium isotopomer, the splitting decreases by two orders of magnitude, as was predicted

Table 7. Spectroscopic ground state constants of the Watson Hamiltonian in *S* reduction for carbodiimide isotopomers.

Constant	HNCNH[a]	$HN^{13}CNH$	$H^{15}NC^{15}NH$	DNCND
A/MHz	379 244.402(21)[b]	378 735.042(19)	375 820.944 5(49)	211 517.168(25)
B/MHz	10 366.940 2(11)	10 367.373 7(20)	9 771.933 0(11)	9 072.434 0(50)
C/MHz	10 366.088 7(12)	10 366.120 4(30)	9 771.184 6(18)	9 066.601 9(60)
D_J/kHz	3.246 24(82)	3.240 8(28)	2.882 5(24)	2.716 9(57)
D_{JK}/kHz	325.790(16)	323.89(23)	315.83(13)	29.988(47)
D_K/MHz	168.625 0(44)	168.625 0[c]	168.625 0[c]	57.792 2(53)
d_1/Hz	−5.678(26)	−5.734 2(67)	−5.665 0(30)	−10.812(37)
d_2/Hz	−16.825(12)	−16.825[c]	−16.825[c]	−25.52(23)
H_{KJ}/Hz	−268.8(25)	−268.8[c]	−268.8[c]	−369.86(43)
H_K/kHz	430.92(40)	430.92[c]	430.92[c]	76.00(14)
h_2/mHz	–	–	–	0.83(11)
L_{KJ}/Hz	5.66(12)	–	–	–
L_K/kHz	1.773(17)	–	–	0.141 6(15)
S_{KJ}/mHz	32.3(23)	–	–	–
S_K/Hz	8.42(35)	–	–	0.193 9(51)
T_{KJ}/mHz	0.468(13)	–	–	–
T_K/mHz	31.7(34)	–	–	–
U_K/μHz	61.(12)	–	–	–
σ[d]/kHz	168	11	15	261
No. of lines	449	33	60	397
κ[e]	−0.999 995 383(12)	−0.999 993 195(20)	−0.999 995 911(12)	−0.999 942 385(70)

[a] Data for the fit of the main species were taken from [1, 4, 5]
[b] The numbers in parentheses are one standard deviation in units of the last digit quoted.
[c] Constant held fixed at the value of the main species.
[d] Standard deviation of the fit.
[e] Ray's asymmetry parameter.

by Pracna *et al.* [3]. The higher mass and the resulting decrease of the zero point energy level are responsible for this effect.

Not only the magnitude of the torsional splitting changes upon isotopic substitution, but also the J dependence: the splitting of the $^rQ_0$-branch transitions of $HN^{13}CNH$ decreases with increasing J, while for all other isotopomers the splitting increases with J. The strong cyanamide absorptions in the region of the $^rQ_1$ branch of DNCND perturb in many cases at least one component of the torsional doublet, so that the errors in the values obtained for the torsional splitting are larger than the J dependence. From the diagram in figure 11, one can only see that the torsional splitting of the $J_{2,J-2} \leftarrow J_{1,J-1}$ branch transitions is somewhat larger than the splitting of the $J_{2,J-1} \leftarrow J_{1,J}$ transitions, which is also true for the main species [5]. The $^rQ_0$- and $^rQ_1$-branch transitions of DNCND show a much smaller J dependence than was found for the other isotopomers.

DNCND is more asymmetric than the other isotopomers, but it still shows an anomalous K_a doubling of the $K_a = 2$ energy levels, which means that the $J_{2,J-2}$ energy levels are below the $J_{2,J-1}$ energy levels. This can be clearly seen in figure 12, where the reduced term values F_{red} of these states are plotted against J. The reduced term values are defined below.

Winnewisser [19, 23] showed that two contributions to the K_a-type doubling are important for accidentally nearly symmetric top molecules: the inertial asymmetry splitting which can be considered to be a $\Delta K_a = \pm 2$ interaction, and the centrifugal-distortion splitting, represented by the $\Delta K_a = \pm 4$ interaction matrix element in the asymmetric top Hamiltonian. The anomalous K_a-type doubling has been discussed by applying a second-order perturbation treatment to Watson's *S*-reduced Hamiltonian [24]. The different contributions to the observed splitting can be visualized by calculating reduced term values F_{red} defined as $F_{red} = F - F_{mod}$ [5]. The term values F were calculated with all constants given in table 7, reproducing the observed spectrum, and the term values F_{mod} were obtained according to three different models:

- F_{mod} is calculated with both the $\Delta K_a = \pm 2$ and $\Delta K_a = \pm 4$ matrix elements fixed to zero, so that F_{mod} represents the term value of DNCND as a

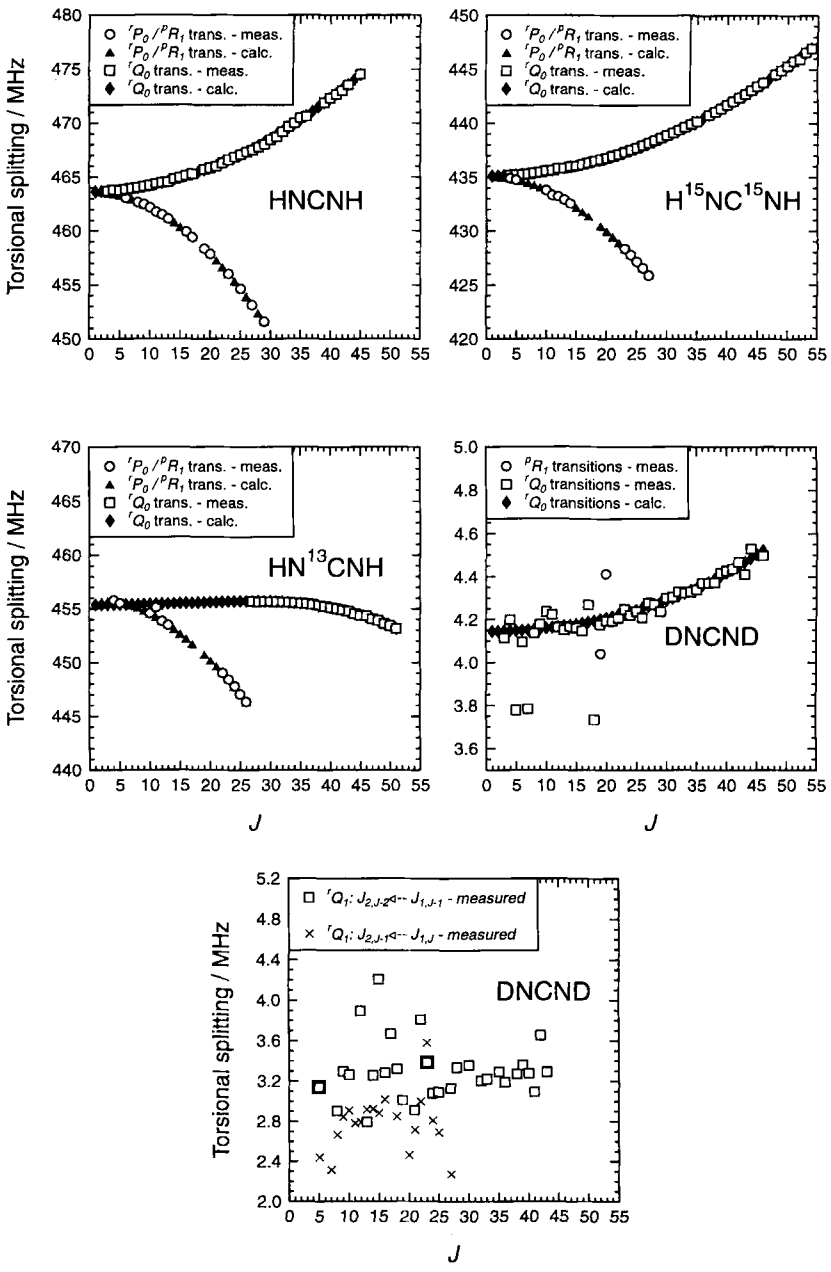

Figure 11. The J dependence of the torsional splittings of the $^rQ_0$ branches of five HNCNH isotopomers. The calculated values of the splittings for the first four species were obtained either with the aid of rotational constants of the Watson Hamiltonian or with the aid of power series constants. Additionally, the measured torsional splittings of the $^rQ_1$-branch transitions of DNCND are displayed. Overlaps with strong cyanamide lines are so serious in this region, that the errors of the splitting are as large as ±1 MHz, and therefore a dependence of the torsional splitting on J cannot be determined.

symmetric top molecule. In this case the difference between two F_{red} values with the same J and K_a quantum numbers is equal to the total observable K_a-type doubling contribution to the energy levels.

- F_{mod} is calculated with the $\Delta K_a = \pm 2$ matrix elements fixed to zero; it contains, however, the $\Delta K_a = \pm 4$ centrifugal distortion contribution to the K_a-type doubling of the transitions. In this case F_{red} reflects the inertial asymmetry contribution to the doubling.
- F_{mod} is calculated with the $\Delta K_a = \pm 4$ matrix elements fixed to zero, but retaining the $\Delta K_a = \pm 2$ inertial asymmetry contribution to the K_a-type doubling of the transitions. In this case F_{red} reflects the centrifugal-distortion contribution to the splitting.

It becomes clear from figure 12 that even for DNCND the $\Delta K_a = \pm 4$ interaction contribution is the dominant term for the K_a doubling of the $K_a = 2$ levels, and that the $\Delta K_a = \pm 2$ and $\Delta K_a = \pm 4$ interactions are of oppo-

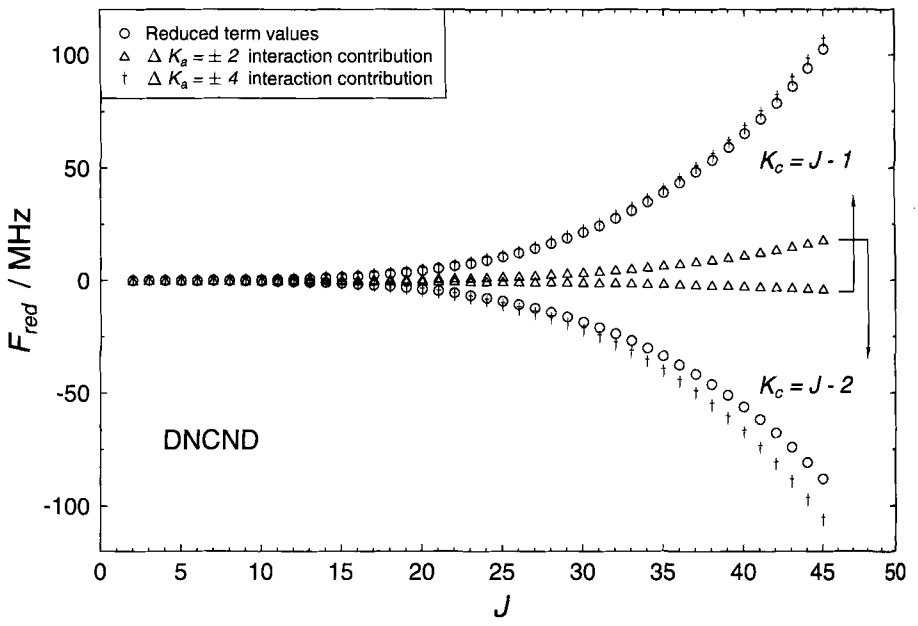

Figure 12. Reduced term values of the $K_a = 1$ and $K_a = 2$ rotational levels of DNCND. The reduced term values are defined as $F_{red} = F - F_{mod}$, where F_{mod} is a term value calculated according to the three different models discussed in the text.

site sign. A comparison with figure 8 in [5] shows that the centrifugal distortion contribution is very similar in HNCNH and DNCND, while the asymmetry contribution is 100 times larger in DNCND.

5. Calculation of the experimental structure

Due to the C_2 symmetry of the HNCNH, the rotational constants of the four isotopomers considered here are sufficient to derive an r_0, r_s and a r_m^ρ structure. For calculating the r_0 structure the least squares fitting program STRFTQ3 written by Schwendeman [25] was used. This program could also calculate pseudo-Kraitchman structures (p-Kr), in which the five independent, geometrically defined coordinates (the HN and CN distances and the HNC, NCN and HN···NH angles) are fitted to differences of either the planar moments (ΔP) or moments of inertia (ΔI). All rotational constants listed in table 7 are included in the fit with the same weight. A generalized correction of the rovibrational contributions to the experimentally determined moments of inertia I_0 was performed following the relation given by Demaison and Nemes [26]:

$$\log \epsilon = \log (I_0 - I_e) = 1.247 \log (I_0 - 2.651) . \quad (7)$$

The so-called Laurie correction [25, 27] was also applied, which takes into account the shrinkage of a bond by substituting an atom with its heavier isotope. The HN distance was reduced by 0.003 Å when a H/D substitution was considered and the CN distance by 0.000 08 Å when one of the heavier atoms was substituted. The results of all the structural fits are reported in table 8.

The high inertial symmetry of carbodiimide, with $B \approx C$, correlated with small b and c coordinates for several atoms, leads to a major problem in the investigation of its r_s structure. The equations given by Nygaard [28] for double substitution produce several imaginary atomic coordinates and are therefore not applicable. However, an r_s structure was successfully calculated with the fitting program RU238 written by Rudolph [29]. The fitting procedure, introduced by Typke [30], provides the advantage of including the centre of mass and the 2nd moment conditions in the fit of the atomic coordinates in the principal axis system (PAS) of the main isotopomer. The program also offers the option of considering the correlation between rotational constants and their experimental accuracies. The Demaison/Nemes correction as well as the Laurie correction have also been applied in the r_s fits. The results are presented in table 8.

Harmony and co-workers [31–34] introduced a method for obtaining near equilibrium structures by using scaled moments of inertia, I_{mg}^ρ, which are calculated according to the formula

$$[I_{mg}^\rho]_\alpha = (2\rho_g - 1)[I_0^g]_\alpha . \quad (8)$$

The scaling factor ρ_g is obtained by

$$\rho_g = \frac{[I_s^g]_1}{[I_0^g]_1} . \quad (9)$$

$[I_0^g]_1$ is the experimentally determined ground state moment of inertia of the parent species about the g axis, $g \in \{a, b, c\}$, and I_s^g is the corresponding substitution moment of inertia computed from the atomic substitution coordinates resulting from the r_s fit. The index α numbers the available isotopomers. After the determi-

Table 8. Internuclear distances and bond angles of HNCNH, calculated using different models.

Nr.	Method		$r_{(NH)}$ /Å	$r_{(CN)}$ /Å	∠HNC /°	∠NCN /°	∠HN···NH/°
1	r_0		1.003 9(d)[d]	1.224 7(2)	119.10(7)	171.6(2)	89.35(9)
2	r_0	DEM./NEM.[e]	1.001 1(7)	1.221 2(3)	119.0(1)	171.6(4)	89.3(1)
3	r_0	LAURIE[f]	1.007 9(3)	1.223 7(1)	119.53(7)	172.7(2)	89.75(8)
4	r_0	DE./NE.[e]+LA.[f]	1.005 1(4)	1.220 3(2)	119.38(8)	172.6(3)	89.7(1)
5	r_0	p − Kr, ΔP	1.005(4)	1.223(1)	119.2(9)	172.0(2)	89.6(4)
6	r_0	p − Kr, ΔI	1.004(3)	1.223(1)	119.3(7)	172.0(2)	89.6(4)
7	r_s[a]		1.007 416(2)	1.224 136(9)	118.634(4)	170.66(1)	89.10(1)
8	r_s[b]		1.007 41(2)	1.224 15(1)	118.638(2)	170.631(2)	88.99(3)
9	r_s[c]		1.007 37(9)	1.224 22(4)	118.635(8)	170.630(4)	88.986(5)
10	r_s[c]	DEM./NEM.[e]	1.004 86(9)	1.219 75(4)	118.550(8)	170.602(4)	88.982(5)
11	r_s[c]	LAURIE[f]	1.012 7(1)	1.225 33(5)	118.630(9)	170.806(5)	89.146(6)
12	r_s[c]	DE./NE.[e]+LA.[f]	1.010 14(9)	1.220 86(4)	118.544(8)	170.778(4)	89.141(5)
13	r_m^ρ		1.013 5(6)	1.222 8(2)	118.28(9)	171.2(3)	88.8(1)
14	r_m^ρ	BER./HARM.[g]	1.014 6(3)	1.222 8(1)	118.41(4)	170.7(2)	88.74(6)
15	r_e	*ab + initio*[h]	1.009 2	1.223 1	118.26	170.62	89.18

[a] r_s fit without considering centre of mass and 2nd moment conditions. Rotational constants are assumed to be uncorrelated.
[b] r_s fit including centre of mass and 2nd moment conditions. Rotational constants are assumed to be uncorrelated.
[c] r_s fit including centre of mass and 2nd moment conditions. Correlations between the rotational constants are considered.
[d] The numbers in parentheses are one standard deviation in units of the last digit quoted.
[e] Empirical correction of rovibrational effects according to Demaison and Nemes [26].
[f] Laurie correction [27].
[g] Correction of large vibration–rotation effects of deuterium according to Berry and Harmony [32, 35].
[h] [6].

nation of the I_{mg}^ρ values for all four isotopomers the data were then used to calculate the r_m^ρ structure with the aid of Schwendeman's [25] program. For molecules containing hydrogen, the I_m^ρ values obtained for the isotopomers involving H/D substitution are generally unreliable, and their utilization along with the I_m^ρ values of the heavy atom isotopomers lead to poor X–H parameters and degrade the heavy atom parameters [32]. To account for the imperfect scaling in these cases the I_{mg}^ρ values for a D-substituted species are corrected by an amount Δ_g equivalent to an elongation δr of the C–D internuclear distance by an amount $\delta r = 0.0028$ Å[35]. If two equivalent hydrogen atoms are replaced by two deuterium atoms, the correction for I_m^ρ about the a axis is

$$(I_{ma}^\rho)_{\text{corr}}^{\text{D}} - (I_{ma}^\rho)^D = \Delta_a = \pm 2 m_{\text{D}} \sum_{i=1}^{2} (b_i \delta b_i + c_i \delta c_i). \quad (10)$$

b_i, c_i and δb_i, δc_i are, respectively, the coordinates of the ith deuterium atom and the components of $\delta \mathbf{r}$. Similar equations apply for the other axes, and the plus or minus sign is selected according to whether $\rho_g < 1$ or $\rho_g > 1$. For calculating the I_{mg}^ρ values the I_s values were used, which were obtained taking into account the centre of mass, the 2nd moment condition, and correlation between the rotational constants. This fit is designated by r_s^c (number 9) in table 8. The resulting r_m^ρ structures, with and without the described correction, are included in table 8 (numbers 13 and 14).

For comparison with all these approches to an experimental structure, the *ab initio* r_e–structure [6], extrapolated for an infinitely large basis set, is also listed in table 8 (number 15).

6. Discussion of the HNCNH structures

As mentioned above, the most serious problems in determining the experimental structure of HNCNH are encountered for the small coordinates of the nitrogen and carbon nuclei in the principal axis system of the main species. The carbon nucleus, lying on the C_2-symmetry axis, shows a b coordinate of 0.0431 Å, and the absolute values of the b and c coordinates of the nitrogen nuclei are 0.0568 Å and 0.0565 Å, respectively. The critical limit for the determination of a substitution coordinate with still significant accuracy is given as ≈ 0.12 Å by Rudolph [29]. This means that three of the seven coordinates which have to be determined for the HNCNH structure are below this limit. It has been observed that small coordinates can lead to non-converging r_s fits [30]. Nevertheless, in the case of carbodiimide all r_s fits converged. The corrections of the atomic coordinates in the last iteration step were smaller than

10^{-14} Å even for the fit designated r_s^a in table 8 (number 7), where the centre of mass and 2nd moment conditions were not considered. The effect in the small coordinates can only be seen directly in the pseudo-Kraitchman fits. The structural parameters of those fits show statistical errors which are approximately one order of magnitude larger than for the other fits.

Because the number of equations is equal to the number of variables to be determined in the r_s^a fit, the errors given result from propagation of the experimental error. For all other fits the number of equations is larger than the number of variables. However, the r_s structural parameters do not change substantially upon including the centre of mass and 2nd moment conditions. This indicates that the small atomic coordinates are not critical for the determination of an r_s structure by the fitting method in this specific case. Nevertheless, the Costain errors $\sigma_{(x)}$, which are given by $\sigma_{(x)} = K/x$, where x is the coordinate in the PAS of the main species and K a 'constant' given by van Eijck [36], are large. Propagation of σ_x to the internuclear distances and angles result in: $\delta(r_{NH}) = 0.0168$ Å, $\delta(r_{NC}) = 0.0025$ Å, $\delta(\angle HNC) = 1.65°$, $\delta(\angle NCN) = 2.50°$ and $\delta(\angle HN\cdots NH) = 3.75°$. These errors are in most cases much larger than the differences between the structures resulting from all applied models. However, the Costain formula for the uncertainty in the coordinate x is obtained under the assumption that one factor in Kraitchman's equations dominates the uncertainty of x, namely, the factor which does not depend on a difference of planar moments in the denominator. This is not necessarily true in the case of small coordinates.

The basic assumption of the r_m^ρ method is that the ratio between the substitution moment of inertia I_s^g about the g axis and the corresponding experimentally determined moment of inertia I_0^g is nearly constant within a few parts in 10^{-4} for all isotopomers [31]. Table 9 gives the described ratio for all investigated HNCNH isotopomers. The numbers in the table indicate that the condition for the r_m^ρ method is fulfilled for all but the $[I_s^a]_D/[I_0^a]_D$ ratio. After applying the correction given by equation (13) the heavy atom distance, i.e. the CN distance, should therefore approximate the true r_e value within 0.002 Å [34]. This accuracy is supported by the excellent agreement between the $(r_m^\rho)_{corr}$ value and the *ab initio* calculation. According to Helgaker *et al.* [37] the r_e distances obtained by the cc-pVQZ CCSD(T) *ab initio* method should also be in error of about 0.0022 Å. The agreement between the $(r_m^\rho)_{corr}$ and the *ab initio* structure in the case of the second heavy atom parameter, the NCN angle, is also satisfying. On the other hand, it was stated that the $(r_m^\rho)_{corr}$ X–H distances of polyatomic organic molecules cannot be relied upon as good approximations to r_e values. They remain sensitive to the inadequacies of the scaling and correction procedures which probably cannot account for the large vibration–rotation effects in light atoms, especially those undergoing large-amplitude, low-frequency motions [33], as in carbodiimide. Therefore, the relatively large difference of 0.0054 Å between the $(r_m^\rho)_{corr}$ and *ab initio* value of the HN distance is not surprising. In this case the agreement between the r_s structure, with the application of the Demaison/Nemes and Laurie correction (number 12 in table 8), and the *ab initio* calculation is within the stated error of 0.0022 Å, which is also true for the CN distance.

However, Rudolph [29] emphasized that the Demaison/Nemes relation was not meant to be directly applicable to large molecules. The Laurie corrections suffer from the fact that rules for the effects of isotopic substitution on bond angles have not been given and probably do not exist [25]. In addition, the effect of using corrections for average internuclear distances has not been assessed. For these reasons the Laurie correction is most useful for assessing uncertainties [25]. We therefore chose the r_s structure which takes into account the centre of mass, the second moment condition, and the correlation of the rotational constants, as our best experimental approximation to the r_e structure (number 9 in table 8): $r_{NH} = 1.0074$ Å, $r_{CN} = 1.2242$ Å, $\angle HNC = 118.63°$, $\angle NCN = 170.63°$, $\angle HN\cdots NH = 88.99°$. The number of digits quoted allow for errors with two significant figures according to the recommendations of Taylor *et al.* [38]. Considering the differences in the various r_s structural parameters of table 8 as a basis for assessing the errors, we conclude that the errors of the internuclear distances are in the range from 0.002 to 0.01 Å and the errors of the bond angles in the range

Table 9. Ratio $I_s^g : I_0^g$ for all investigated HNCNH isotopomers.

Isotopomer α	$\frac{[I_a^s]_\alpha}{[I_a^0]_\alpha}$	$\frac{[I_a^s]_1}{[I_a^0]_1} - \frac{[I_a^s]_\alpha}{[I_a^0]_\alpha}$	$\frac{[I_b^s]_\alpha}{[I_b^0]_\alpha}$	$\frac{[I_b^s]_1}{[I_b^0]_1} - \frac{[I_b^s]_\alpha}{[I_b^0]_\alpha}$	$\frac{[I_c^s]_\alpha}{[I_c^0]_\alpha}$	$\frac{[I_c^s]_1}{[I_c^0]_1} - \frac{[I_c^s]_\alpha}{[I_c^0]_\alpha}$
HNCNH	1.017871	0	0.998163	0	0.998319	0
HN^{13}CNH	1.017873	$-0.02/10^4$	0.998205	$-0.42/10^4$	0.998359	$-0.40/10^4$
H^{15}NC^{15}NH	1.017710	$1.61/10^4$	0.998274	$-1.11/10^4$	0.998424	$-1.05/10^4$
DNCND	1.009910	$79.61/10^4$	0.998393	$-2.30/10^4$	0.998533	$-2.14/10^4$

Table 10. Comparison of molecular structures of related imines.

Structural parameter		HN=CH_2 [39]	HN=C=CH_2 *ab initio* [40]	HN=C=NH This work	HN=C=O [41]
r_{NH}	/Å	1.021	1.017	1.0074	0.9946
r_{CN}	/Å	1.273	1.234	1.2242	1.2140
∠HNC	/°	110.4	115.4	118.63	123.9
∠XCN	/°	–	174.6	170.63	172.6

from 0.1 to 0.2°. Errors of this magnitude are normally expected for an r_s structure [29].

In order to understand the structure of HNCNH in the context of simple models we collected the structural parameters of related molecules with an imine group in table 10. They are listed in a sequence showing a shrinkage of the HN bond and also a shrinkage of the CN bond, while the HNC angle is opened. Going from methanimine (H_2CNH) to ketenimine (H_2C_2NH) a second π system is introduced with which the lone pair of the nitrogen can interact. Because of this interaction the CCN skeleton is not linear, which might have been expected for a system which is isoelectronic with the allene molecule. The nitrogen moves towards the second π-bond system, forming a CCN angle smaller than 180° and a larger HNC angle. Substitution with the more electronegative NH or O groups intensifies the interaction, leading to even stronger NH and CN bonds in carbodiimide and isocyanic acid, both of which exhibit spectra showing indications of large amplitude motions.

The authors thank Dr M. Lock and G. Mellau for help with the FTIR measurements, Dr Th. Klaus with some millimetre wave measurements and Dr B. P. Winnewisser for many helpful discussions during the analysis of the data and for critically reading the manuscript. W. Jabs thanks the Studienstiftung des deutschen Volkes for a scholarship, the members of the Cologne submillimetre wave laboratory for their friendly collaboration, and Professor J. Koput for many discussions about *ab initio* calculations. The work in Gießen was supported in part by the Deutsche Forschungsgemeinschaft and Fonds der Chemischen Industrie, while the work in Cologne was supported in part by the Deutsche Forschungsgemeinschaft via Grant SFB 301 and special funding from the Science Ministry of the Land Nordrhein–Westfalen.

References

[1] Birk, M., Winnewisser, M., and Cohen, E. A., 1989, *J. molec. Spectrosc.*, **136,** 402.
[2] Winnewisser, M., and Birk, M., 1988, *J. chem. Soc., Faraday Trans. 2*, **84,** 1341.
[3] Pracna, P., Winnewisser, M., and Winnewisser, B. P., 1993, *J. molec. Spectrosc.*, **162,** 127.
[4] Wagener, V., Winnewisser, M., and Bellini, M., 1995, *J. molec. Spectrosc.*, **170,** 323.
[5] Jabs, W., Winnewisser, M., Belov, S. P., Klaus, T., and Winnewisser, G., 1997, *Chem. Phys.*, **225,** 77.
[6] Koput, J., Jabs, W., and Winnewisser, M., 1998, *Chem. Phys. Lett.*, **295,** 462.
[7] Moruzzi, G., Jabs, W., Winnewisser, B. P., and Winnewisser, M., 1998, *J. molec. Spectrosc.*, **190,** 353.
[8] Winnewisser, G., Krupnov, A. F., Tretyakov, M. Y., Liedtke, M., Lewen, F., Saleck, A. H., Schieder, R., Shkaev, A. P., and Volokhov, S. V., 1994, *J. molec. Spectrosc.*, **165,** 294.
[9] Winnewisser, G., 1995, *Vib. Spectrosc.*, **8,** 241.
[10] Belov, S. P., Lewen, F., Klaus, T., and Winnewisser, G., 1995, *J. molec. Spectrosc.*, **174,** 606.
[11] Fletcher, W. H., and Brown, F. B., 1963, *J. chem. Phys.*, **39,** 2478.
[12] Birk, M., 1988, Dissertation, Justus-Liebig-Universität Gießen, Germany.
[13] Winnewisser, M., Lichau, H., and Wolf, F., 1999, in preparation.
[14] Maiwald, F., Lewen, F., Vowinkel, B., Jabs, W., Paveljev, D. G., Winnewisser, M., and Winnewisser, G., 1999, *IEEE Microwave Guided Wave Lett.*,submitted.
[15] Guelachvili, G., and Rao, K. N., 1986, *Handbook of Infrared Standards* (London: Academic Press, Inc.).
[16] Schermaul, R., 1996, Dissertation, Justus-Liebig-Universität Gießen, Germany.
[17] Hougen, J. T., 1984, *Can. J. Phys.*, **62,** 1392.
[18] Bunker, P. R., 1979, *Molecular Symmetry and Spectroscopy* (San Diego, California 92101: Academic Press, Inc.).
[19] Winnewisser, G., 1972, *J. chem. Phys.*, **56,** 2944.
[20] Stroh, F., Winnewisser, M., and Winnewisser, B. P., 1993, *J. molec. Spectrosc.*, **162,** 435.
[21] Watson, J. K. G., 1967, *J. chem. Phys.*, **46,** 1935.
[22] Watson, J. K. G., 1968, *J. chem. Phys.*, **48,** 4517.
[23] Winnewisser, G., 1972, *J. chem. Phys.*, **57,** 1803.
[24] Yamada, K. M. T., Behrend, J., Belov, S. P., and Winnewisser, G., 1996, *J. molec. Spectrosc.*, **176,** 397.
[25] Schwendeman, R. H., 1974, *Critical Evaluation of Chemical and Physical Structural Information*, edited by D. R. Lide Jr and M. A. Paul (Washington DC: National Academy of Science), pp. 94–115.
[26] Demaison, J., and Nemes, L., 1979, *J. molec. Struct.*, **55,** 295.
[27] Laurie, V. W., and Herschbach, D. R., 1962, *J. chem. Phys.*, **37,** 1687.
[28] Nygaard, L., 1976, *J. molec. Spectrosc.*, **62,** 292.

[29] RUDOLPH, H. D., 1995, *Advances in Molecular Structure Research*, Vol. 1, edited by I. Hargittai and M. Hargittai (Greenwich, CT: JAI Press Inc.), pp. 63–114.
[30] TYPKE, V., 1978, *J. molec. Spectrosc.*, **69,** 173.
[31] HARMONY, M. D., and TAYLOR, W. H., 1986, *J. molec. Spectrosc.*, **118,** 163.
[32] BERRY, R. J., and HARMONY, M. D., 1990, *Struct. Chem.*, **1,** 49.
[33] TAM, H. S., CHOE, J.-I., and HARMONY, M. D., 1991, *J. phys. Chem.*, **95,** 9267.
[34] HARMONY, M. D., 1992, *Acc. Chem. Res.*, **25,** 321.
[35] HARMONY, M. D., 1990, *J. chem. Phys.*, **93,** 7522.
[36] VAN EIJCK, B. P., 1982, *J. molec. Spectrosc.*, **91,** 348.
[37] HELGAKER, T., GAUSS, J., JØRGENSEN, P., and OLSEN, J., 1997, *J. chem. Phys.*, **106,** 6430.
[38] TAYLOR, B. N., PARKER, W. H., and LANGENBERG, D. N., 1969, *Rev. mod. Phys.*, **41,** 375.
[39] PEARSON JR, R., and LOVAS, F. J., 1977, *J. chem. Phys.*, **66,** 4149.
[40] RODLER, M., BROWN, R. D., GODFREY, P. D., and KLEIBÖMER, B., 1986, *J. molec. Spectrosc.*, **118,** 267.
[41] YAMADA, K. M. T., 1980, *J. molec. Spectrosc.*, **79,** 323.